Journal of Thermal Biology 84 (2019) 53–73

Contents lists available at ScienceDirect

Journal of Thermal Biology

journal homepage: www.elsevier.com/locate/jtherbio

A study of heat transfer during cryosurgery of lung cancer

Mukesh Kumar[a,*], Subrahamanyam Upadhyay[b], K.N. Rai[3]

[a] DST-CIMS, Institute of Science, Banaras Hindu University, Varanasi, India
[b] Department of Mathematics, Eternal University, Solan (H.P.), India
[3] Department of Mathematical Sciences, IIT(BHU), Varanasi, India

ARTICLE INFO

Keywords:
Cryosurgery
DPL model
FEM
Generalized boundary condition
Generalized inverse

ABSTRACT

In this study, a mathematical model describing two-dimensional bio-heat transfer during cryosurgery of lung cancer is developed. The lung tissue is cooled by a cryoprobe by imposing its surface at a constant temperature or a constant heat flux or a constant heat transfer coefficient. The freezing starts and the domain is distributed into three stages namely: unfrozen, mushy and frozen regions. In stage I where the only unfrozen region is formed, our problem is an initial-boundary value problem of the hyperbolic partial differential equation. In stage II where mushy and unfrozen regions are formed, our problem is a moving boundary value problem of parabolic partial differential equations and in stage III where frozen, mushy, and unfrozen regions are formed, our problem is a moving boundary value problem of parabolic partial differential equations. The solution consists of the three-step procedure: (i) transformation of problem in non-dimensional form, (ii) by using finite differences, the problem converted into ordinary matrix differential equation and moving boundary problem of ordinary matrix differential equations, (iii) applying Legendre wavelet Galerkin method the problem is transferred into the generalized system of Sylvester equations which are solved by applying Bartels-Stewart algorithm of generalized inverse. The complete analysis is presented in the non-dimensional form. The consequence of the imposition of boundary conditions on moving layer thickness and temperature distribution are studied in detail. The consequence of Stefan number, Kirchoff number and Biot number on moving layer thickness are also studied in specific.

1. Introduction

Cancer has turned out to be one of the most threatening diseases all over the globe. Presently 90.5 million population is suffering from cancer and as estimated from studies by 2020 around 20 million fresh cancer cases and 10 million cancer deaths will occur annually(World Health Organization). Diet and obesity (30–35 percent), Tobacco (25–30 percent), infections(15–20 percent), radiation (up to 10 percent), mental pressure, less body movement, and pollution are common contributes to cancer death (Islami et al., 2018). However, it is still difficult to specify an exact cause behind a certain type of cancer due to the existence of a large number of factors in environment. for e.g. tobacco is not only a factor for lung cancer, air pollution or radiation also contributes to its growth in human body (Tolar and Neglia, 2003). Cancer mainly effects the lungs, stomach, liver, prostate, and colorectal among all other body parts.

Lung cancer is one amongst the commonly found cancer globally comprising 1.69 million new patients yearly and is cause for 22 percent of total deaths (WHO) due to cancer. Cigarette smoking, second-hand smoke, exposure to radon and air pollution etc are some of its main factors. There is no assured method to intercept lung cancer but danger can be decreased if we: (i) Stop smoking, (ii) Avoid second-hand smoke, (iii) Check our home for radon, (iv) Include fresh fruits and vegetables in our diet, (v) make exercise on the daily routine. Although it can be cured by some therapies too commonly known as cryosurgery, chemotherapy, radiation therapy, and hyperthermia. But amongst these ones of the most important is cryosurgery (Kumar et al., 2018).

Cryosurgery can be stated as the destruction of diseased tissue applying intense cold temperature in surgery (Pasquali, 2015). Here, diseased tissues are injected by an instrument called cryoprobe with liquid nitrogen (Allington, 1950). Cancer cells are frozen with liquid nitrogen or argon gas and by the time killed in the process of cryosurgery. There are several benefits of the cryosurgery such as (i) minimum cost incurred, (ii) minimum pain suffered, (iii) shorter stay in the hospital and (iv) shorter recovery time (Deng and Liu, 2005). In lung cancer, the main objective of cryosurgery is to increase the destruction of tumor tissues while protecting enclosed healthy lung tissues. Cryosurgery is considered to be a beneficial treatment of lung

* Corresponding author.
E-mail addresses: michelmukesh@gmai.com (M. Kumar), subabbu16@gmail.com (S. Upadhyay), knrai.apm@itbhu.ac.in (K.N. Rai).

https://doi.org/10.1016/j.jtherbio.2019.05.023
Received 18 January 2019; Received in revised form 4 May 2019; Accepted 22 May 2019
Available online 03 June 2019
0306-4565/

Nomenclature

x	space coordinate
y	space coordinate
ρ	density(kg/m^3)
c	specific heat(J/kg^0C)
k	thermal conductivity of the tissue(W/m^0C)
a	thermal diffusivity
ρ_b	density of blood(kg/m^3)
c_b	specific heat of blood(J/kg^0C)
w_b	blood perfusion rate(ml/sl)
T	temperature($^\circ C$)
t	time(s)
L	latent heat(kJ/kg)
T_b	arterial temperature($^\circ C$)
T_0	initial temperature($^\circ C$)
T_c	cryoprobe temperature($^\circ C$)
T_l	liquidus temperature($^\circ C$)
T_s	solidus temperature($^\circ C$)
l	length of the tissue
s_i	distance from origin
q	heat flux
Q_m	metabolic heat generation(W/m^3)
τ_q	phase lag in heat flux(s)
τ_T	phase lag in temperature gradient(s)
T_w	surface temperature
T_r	surrounding temperature
h	heat transfer coefficient
erf	error function
$erfc$	complementary error function

Dimensionless variable

X	dimensionless space coordinate
Y	dimensionless space coordinate
Fo	Fourier number or dimensionless time
Fo_q	dimensionless phase lag due to heat flux
Fo_T	dimensionless phase lag due to temperature gradient
λ_i	dimensionless distance
θ	dimensionless temperature
θ_b	dimensionless blood temperature
θ_u	dimensionless unfrozen temperature
θ_m	dimensionless mushy temperature
θ_f	dimensionless frozen temperature
θ_w	dimensionless surface temperature
θ_r	dimensionless surrounding temperature
θ_s	dimensionless solidus temperature
P_f	dimensionless blood perfusion coefficient
P_m	dimensionless metabolic heat source coefficient
Ste	Stefan number
K_i	Kirchoff number
B_i	Biot number

Subscript

u, 1	indication for unfrozen
m, 2	indication for mushy
f, 3	indication for frozen

cancer as it increases the possibilities of longer survival (Kumar et al., 2018). For successful cryosurgical treatment, temperature distribution and positions of phase change interface in lung-tumor tissue are required (Katiyar et al., 2017). The comprehensive study has been presented regarding the rate of cell destruction and temperature distribution in the tumor during cryosurgery (Chua et al., 2007).

Cryosurgical simulation of lung cancer build on systematic freezing time is explored (Tarwidi, 2015). His studies show that temperature distribution and phase change interface position in tissue can be applied to increase destruction to tumor tissue and decrease the injury to normal tissue.

Pennes bio-heat model (Pennes, 1948) has been globally applied by several authors (Kumar et al., 2018; Deng and Liu, 2005; Katiyar et al.,2017; Chua et al., 2007) to answer the phase change heat problem in cryosurgery which is defined as

$$c\rho\frac{\partial T}{\partial t} = -\nabla q + \rho_b w_b c_b (T_b - T) + Q_m \tag{1}$$

where, c and ρ are the specific heat and the density of the tissue, c_b and ρ_b are the specific heat and density of blood, w_b is the blood perfusion rate, q is the heat flux, Q_m is the metabolic heat generation, T is the temperature, T_b is the arterial blood temperature and t is the time.

The above Eqn. (1) is based on Fourier's law which is defined as

$$q(S, t) = -k\nabla T(S, t) \tag{2}$$

where k is the thermal conductivity of the tissue, q(S, t) is the heat flux and T(S, t) is the temperature at position S = (x, y, z).

However, this model concludes the infinite speed of heat and mass propagation. Although in situations dealing with heat and mass transfer in extremely short durations of time, extremely high temperature and moisture gradient, extremely low temperatures and moisture towards absolute zero, or for microscale situations the wave nature of heat and mass propagation become dominant (Kumar et al., 2018). Cattaneo and Vernotte (1958) proposed modified Fourier's and Fick's models (Single phage model) generally called as non-Fourier's and non-Fick's models. For such conditions, a constitutive equation which premises a relaxation time in the heat flux vector q. The single phage model is expressed by

$$q(S, t + \tau_q) = -k\nabla T(S, t),$$

where $\tau_q \neq 0$ is the relaxation time due to heat flux. Using first order Taylor's expansion, the SPL model reduces in the form

$$\left(q + \tau_q \frac{\partial q}{\partial t}\right)(S, t) = -k\nabla T(S, t). \tag{3}$$

There are several studies accessible in the literature (Deng and Liu, 2005; Katiyar et al., 2017; Kumar et al., 2015, 2016; Ahmadikia and Moradi, 2012) where the bio-heat model with freezing is applied. The non-Fourier effect of biological tissue of heat conduction during freezing has been used (Ahmadikia and Moradi, 2012). Further, the physical results provided by bio-heat model are sometimes different (Tzou, 1995). Thus to consider the thermal behavior that is not captured by the Fourier's law, a new model by observing phase lag of temperature and phase lag of heat flux gradient is established (Tzou, 1995). This model is known as dual phase lag model(DPL) and is expressed as

$$q(S, t + \tau_q) = -k\nabla T(S, t + \tau_T),$$

where $\tau_q \neq 0$ and $\tau_T \neq 0$ are the relaxation time in heat propagation. Using first order Taylor's expansion, the reduced form of DPL model is

$$\left(q + \tau_q \frac{\partial q}{\partial t}\right)(S, t) = -k\nabla\left(T + \tau_T \frac{\partial T}{\partial t}\right)(S, t). \tag{4}$$

Eq. (4) is called the dual phase lag constitutive relation. From Eqs. (1) and (4) we obtain the below equation:

$$\tau_q c\rho\frac{\partial^2 T}{\partial t^2} + (c\rho + \rho_b w_b c_b \tau_q)\frac{\partial T}{\partial t} =$$
$$k\nabla^2\left(T + \tau_T\frac{\partial T}{\partial t}\right)(S, t) + \rho_b w_b c_b (T_b - T) + Q_m \quad (5)$$

The above equation is known as a dual phase lag(DPL) bio-heat equation.

Many researchers (Majchrzak, 2010; Liu and Chen, 2009; Zhang, 2009; Zhou et al., 2009) have applied Dual-phase lag bio-heat conduction model without phase change. DPL model is suggested to analyse the non-Fourier heat conduction (Antaki, 2005). Zhou et al. (2009) concluded that the thermal behavior of the DPL bio-heat model varies from the other bio-heat models. Similarly, Kumar et al.(2015) investigated the temperature behavior in biological tissues during hyperthermia treatment by using the DPL model. Ahmadikia and Moradi (2012) considered the freezing process in biological tissue with metabolic heat generation and blood flow by applying one-dimensional DPL model. Recently, Kumar et al.(2018) have also used one-dimensional DPL model to study the temperature distribution and moving layer thickness during cryosurgery of lung cancer.

For a real study of lung cancer using cryosurgery, a two-dimensional mathematical bio-heat transfer model is required. In a series of papers Katiyar et al. (2017) studied two-dimensional bio-heat transfer models [Fourier model, SPL model, and DPL model] during cryosurgery of lung cancer when tumor tissue is cooled by a cryoprobe with constant temperature. They solved these problems by enthalpy based finite difference method. A mathematical model during cryosurgery of lung cancer at stage1 is a two-dimensional boundary value problem in presence of lagging time (relaxation time τ_q and τ_T) and a DPL bio-heat transfer model is appropriate. In stage 2 and 3, it will be a moving boundary problem in absence of lagging time and a Fourier bio-heat transfer model is appropriate. To the best of our knowledge, this type of mathematical model is not considered yet.

The aim of our study is to determine how the freezing appears in three stages when lung tissue cooled by a cryoprobe by imposing on it a constant temperature or a constant heat flux or a constant heat transfer coefficient, i.e. by imposing on it the boundary condition of first kind or second kind or third kind. We see how the moving layer thickness and temperature distribution changes as the boundary condition changes. We studied the two-dimensional process of freezing in three various regions: unfrozen region, mushy region, and frozen region. The frequency of heat transfer decides the frequency of tissue cooling. As the aim is to damage the tissues, it is necessary to obtain the rapid cooling rate (Paola, 2015). In the tumor, the freezing interface accelerates as it moves from tumor-tissue into the normal lung tissue (Bischof et al., 1992). Cryosurgical process is simulated mathematically as the equations of heat transfer in liquid and solid phases, where the mushy region (interface region) between two phases is subject to Interface condition (Kotova et al., 2016).

1.1. Formulation of the problem

We observe a lung tissue occupied in the domain $\omega = [(x, y): 0 \le x \le l, 0 \le y \le l]$ in which a tumor tissue of dimension $\omega_t = [(x, y): 0 \le x \le a, 0 \le y \le a]$ is fixed. A cryoprobe is positioned at $x = 0$, $dcm \le y \le ecm$. The lung tissue freezed by a cryoprobe by keeping it at a persistent temperature or a persistent heat flux or a persistent heat transfer coefficient. The freezing begins and the complete procedure of freezing is controlled in three stages. In stage I, the cryoprobe surface is cooled from the initial temperature $T_0(37^0C)$ to liquidus temperature $T_l(-1^0C)$. In this stage, unfrozen region is formed. Further, in stage II the cryoprobe is perpetually cooled from the liquidus temperature T_l to solidus temperature $T_s(-8^0C)$. Throughout this stage, unfrozen region and mushy region co exist at the same time. In stage III, when the temperature of the cryoprobe is perpetually reduced with time the freezing begins from the origin and spreads in the positive x direction. In this stage, unfrozen region, mushy region, and frozen region are set up. The present problem can be described in the given Fig. 1.

The temperature distribution of the tissue is above -1^0C in stage I and during freezing, the relaxation time plays the crucial role and due to this non-Fourier model(DPL) is considered (Kumar et al., 2016). While the Fourier model is used in Stage II and III. From our calculations, we see that the effect of relaxation time is negligible in the mushy and frozen region and present only in unfrozen region.The following presumptions are examined to solve the two-dimensional mathematical model:

(i) Non-Fourier heat conduction law followed by Heat conduction

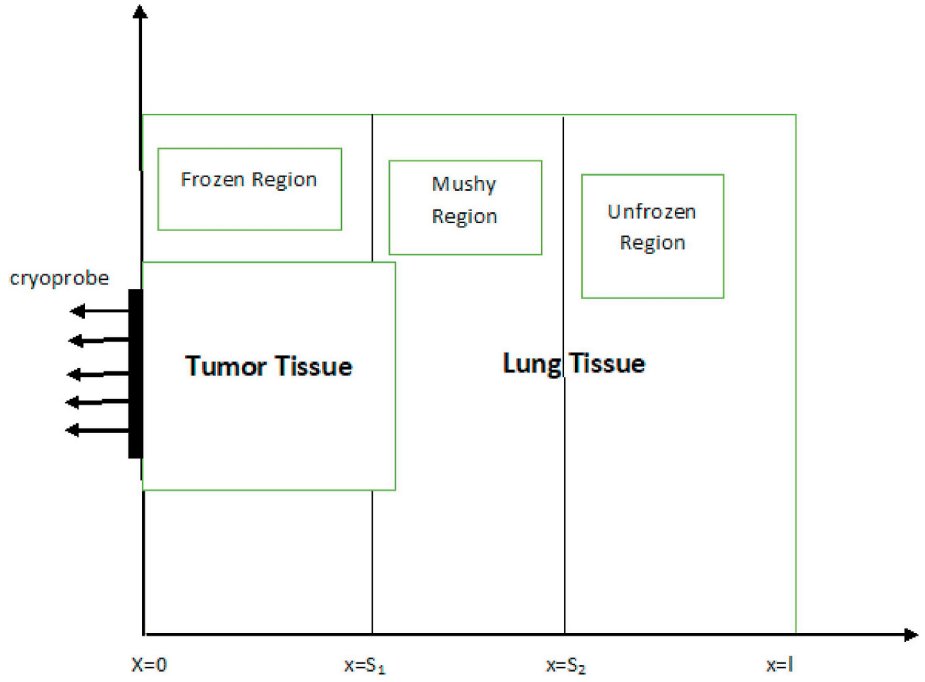

Fig. 1. Schematic of freezing a tumor within the lung.

(Budman et al., 1995).

(ii) When tissue is unfrozen heat source seems due to blood perfusion and metabolism (Deng and Liu, 2005; Frayn, 1996).

(iii) Flawless property of tissues is manipulated with liquidus(upper phase) and solidus(lower phase) temperature as -1^0C and -8^0C respectively (Rabin and Shitzer, 1995).

(iv) The primary(initial) temperature of the tissue is examined as an arterial temperature (37^0C).

(v) Thermophysical properties vary at the point of complete phase change from liquid to solid (Lee and Bastacky, 1995).

(vi) As the solid continuously forms within the intermediate zone, the latent heat of fusion is released accordingly. The heat of fusion can be treated as internal heat generation A within the mushy region (Kumar et al., 2018; Chua et al., 2007; Yadav et al., 2016) is defined as:

$$A = \rho * L\frac{\partial f_s}{\partial t} \tag{6}$$

where f_s is solid fraction present in mushy region.

(vii) The rate of change of solid fraction with respect to time in the mushy region provides a heat generation effect. An exact mathematical expression for the solid fraction cannot be given but the approximate mathematical model is proposed by Gupta (2003) for the numerical solution of the problem and defined as

$$f_s = \frac{f_{su}(T_l - T_m) - f_{su1}(T_s - T_m)}{T_l - T_s} \tag{7}$$

where f_{su} and f_{su1} are solid fractions present at liquid-mush and solid-mush boundaries respectively. At the liquid-mush boundary f_{su} taken as unity and $f_{su1} = 0$, and at the solid-mush boundary f_{su1} taken as unity and $f_{su} = 0$. So, In this paper we have considered that the solid fraction is also present at the liquid-mush boundary.

(viii) Perfect thermal contact is assumed between the probe surface and the adjacent medium.

The mathematical model governing the action of heat transfer comes out in three stages are as follows:

Stage I

$$\rho_u c_u\left(\frac{\partial T_u}{\partial t_1} + \tau_q\frac{\partial^2 T_u}{\partial t_1^2}\right) = k_u\left(\frac{\partial^2 T_u}{\partial x^2} + \frac{\partial^2 T_u}{\partial y^2}\right) + \tau_T k_u\left(\frac{\partial^3 T_u}{\partial t_1 \partial x^2} + \frac{\partial^3 T_u}{\partial t_1 \partial y^2}\right) + \rho_b c_b w_b\left(T_b - T_u - \tau_q\frac{\partial T_u}{\partial t_1}\right) + Q_m,\ 0 < x, y < l,\ t_1 > 0 \tag{8}$$

Initial and boundary condition are given as:

$$T_u(x, y, 0) = T_0, \tag{9}$$

$$\frac{\partial T_u}{\partial t}(x, y, 0) = 0, \tag{10}$$

$$\frac{\partial T_u}{\partial x}(l, y, t_1) = 0, \tag{11}$$

$$\frac{\partial T_u}{\partial y}(x, l, t_1) = 0. \tag{12}$$

Stage II

$$\rho_m c_m\frac{\partial T_m}{\partial t_2} = k_m\left(\frac{\partial^2 T_m}{\partial x^2} + \frac{\partial^2 T_m}{\partial y^2}\right) + A,\ 0 < x, y < s_2,\ t_2 > t_1 \tag{13}$$

$$\rho_u c_u\frac{\partial T_u}{\partial t_2} = k_u\left(\frac{\partial^2 T_u}{\partial x^2} + \frac{\partial^2 T_u}{\partial y^2}\right),\ s_2 < x, y < l \tag{14}$$

Initial and boundary condition are given as:

$$T_m(x, y, t_1^*) = T_u(x, y, t_1^*), \tag{15}$$

$$\frac{\partial T_m}{\partial x}(l, y, t_1) = 0, \tag{16}$$

$$\frac{\partial T_m}{\partial y}(x, l, t_1) = 0, \tag{17}$$

$$T_u(s_2, t_2) = T_m(s_2, t_2) = T_l \tag{18}$$

Interface condition is given by:

$$k_m\frac{\partial T_m}{\partial x} - k_u\frac{\partial T_u}{\partial x} = \rho * Lv_n. \tag{19}$$

where $t_2 = t_1 - t_1^*$

Stage III

$$\rho_f c_f\frac{\partial T_f}{\partial t_3} = k_f\left(\frac{\partial^2 T_f}{\partial x^2} + \frac{\partial^2 T_f}{\partial x^2}\right),\ 0 < x, y < s_1,\ t_3 > t_2 \tag{20}$$

$$\rho_m c_m\frac{\partial T_m}{\partial t_3} = k_m\left(\frac{\partial^2 T_m}{\partial x^2} + \frac{\partial^2 T_m}{\partial y^2}\right) + A,\ s_1 < x, y < s_2 \tag{21}$$

$$\rho_u c_u\frac{\partial T_u}{\partial t_3} = k_u\left(\frac{\partial^2 T_u}{\partial x^2} + \frac{\partial^2 T_u}{\partial y^2}\right),\ s_2 < x, y < l \tag{22}$$

Initial and boundary condition are given as:

$$T_f(x, y, t_2^*) = T_m(x, y, t_2^*) = T_u(x, y, t_2^*), \tag{23}$$

$$\frac{\partial T_f}{\partial x}(l, y, t_1) = 0, \tag{24}$$

$$\frac{\partial T_f}{\partial y}(x, l, t_1) = 0, \tag{25}$$

$$T_f(s_1, t_3) = T_m(s_1, t_3) = T_s, \tag{26}$$

$$T_u(s_2, t_3) = T_m(s_2, t_3) = T_l \tag{27}$$

Interface condition are given by:

$$k_f\frac{\partial T_f}{\partial x} - k_m\frac{\partial T_m}{\partial x} = \rho * Lv_n \tag{28}$$

$$k_m\frac{\partial T_m}{\partial x} - k_u\frac{\partial T_u}{\partial x} = \rho * Lv_n. \tag{29}$$

where $t_3 = t_2 - t_2^*$ and subscripts u, m, f and b denotes unfrozen, mushy, frozen and blood, T is the temperature, t is the time, Q_m is the metabolic heat generation, τ_q and τ_T are the relaxation times.

1.2. General boundary conditions

Due to existence of cryoprobe at surface $x = 0$ the tissue is cooled under generalized boundary condition is as follows:

$$A_o\frac{\partial T}{\partial x}(0, y, t) + B_o T(0, y, t) = f(y, t) \tag{30}$$

I kind:

$$A_o = 0,\ B_o = 1,\ f(t) = T_w \tag{31}$$

II kind:

$$A_o = -k,\ B_o = 0,\ f(t) = q_w \tag{32}$$

III kind:

$$A_o = -k,\ B_o = -h,\ f(t) = -hT_s \tag{33}$$

Continuity of heat flux and temperature at lung-tumor boundary is given as

$$k_t \frac{\partial T_t}{\partial x}(x, y, t) = k_l \frac{\partial T_l}{\partial x}(x, y, t)$$
$$T_t = T_l \tag{34}$$

where, subscripts t and l stands for tumor and normal lung tissue, respectively.

Thermal properties of tumor and healthy lung tissues are different (Bischof et al., 1992; Deng and Liu, 2005). Thermophysical properties of healthy lung and tumor tissue (Kumar and Katiyar, 2016) are taken as

$$k = \begin{cases} k_f, & T < T_l \\ \frac{1}{2}(k_f + k_u), & T_l \le T \le T_s, \\ k_u, & T > T_s \end{cases}$$
$$\rho = \begin{cases} \rho_f, & T < T_l \\ \frac{1}{2}(\rho_f + \rho_u), & T_l \le T \le T_s, \\ \rho_u, & T > T_s \end{cases}$$
$$c = \begin{cases} c_f, & T < T_l \\ \frac{1}{2}(c_f + c_u), & T_l \le T \le T_s. \\ c_u, & T > T_s \end{cases}$$

2. Dimensionless analysis

We define some dimensionless variable and similarity criteria as follows

$$X = \frac{x}{l},\ Y = \frac{y}{l},\ S = \frac{s}{l},\ S_1 = \frac{s_1}{l},\ S_2 = \frac{s_2}{l},\ \theta_s = \frac{T_o - T_s}{T_o - T_l},\ \theta_w = \frac{T_o - T_w}{T_o - T_l},$$
$$\theta_r = \frac{T_o - T_r}{T_o - T_l},\ \theta_b = \frac{T_o - T_b}{T_o - T_l},\ F_0 = \frac{kt}{\rho * cl^2},\ Fo_q = \frac{k\tau_q}{\rho * cl^2},\ Fo_T = \frac{k\tau_T}{\rho * cl^2},$$
$$P_f^2 = \frac{c_b w_b l^2}{k},\ P_m = \frac{Q_m l^2}{k(T_o - T_l)},\ k_{um} = \frac{k_u}{k_m},\ k_{mf} = \frac{k_m}{k_f},\ a_1 = \frac{k_u}{\rho * c_1},\ a_2 = \frac{k_m}{\rho * c_2}$$
$$, a_3 = \frac{k_f}{\rho * c_3},\ Ste_2 = c_m\left(\frac{T_o - T_l}{L}\right),\ Ste_3 = c_f\left(\frac{T_l - T_s}{L}\right),\ Ki = \frac{q_w l}{(T_o - T_l)k_u},\ B$$
$$i = \frac{hl}{k_u},\ \lambda_j(Fo_i) = \frac{s_j(t_i)}{l},\ j = 1{,}2,\ i = 2{,}3,$$
$$A_1 = \frac{A_o(T_o - T_l)}{l},\ B_1 = B_o(T_o - T_l),\ g(F_o) = f(t) - B_o(T_o - T_l).$$

Using these dimensionless variable our problem can be reduce in the following form:

Stage I

$$Fo_q \frac{\partial^2 \theta_u}{\partial Fo_1^2} + (1 + P_f^2 Fo_q)\frac{\partial \theta_u}{\partial Fo_1} = \left(\frac{\partial^2 \theta_u}{\partial X^2} + \frac{\partial^2 \theta_u}{\partial Y^2}\right)$$
$$+ Fo_T \frac{\partial}{\partial F_0}\left(\frac{\partial^2 \theta_u}{\partial X^2} + \frac{\partial^2 \theta_u}{\partial Y^2}\right) + P_f^2(\theta_b - \theta_u) + P_m,\ 0 < X, Y < 1 \tag{35}$$

Initial and boundary condition are given as:

$$\theta_u(X, Y, 0) = 0 \tag{36}$$

$$\frac{\partial \theta_u}{\partial F_0}(X, Y, 0) = 0 \tag{37}$$

$$\frac{\partial \theta_u}{\partial X}(1, Y, Fo_1) = 0 \tag{38}$$

$$\frac{\partial \theta_u}{\partial Y}(X, 1, Fo_1) = 0 \tag{39}$$

where

$$\theta_u = \frac{T_o - T_u}{T_o - T_l}$$

Stage II

$$\left(1 + \frac{1}{Ste_2}\right)\frac{\partial \theta_m}{\partial Fo_2} = \frac{\partial^2 \theta_m}{\partial X^2} + \frac{\partial^2 \theta_m}{\partial Y^2},\ 0 < X, Y < \lambda_2(Fo_2) \tag{40}$$

$$\frac{\partial \theta_u}{\partial Fo_2} = a_{12}\left(\frac{\partial^2 \theta_u}{\partial X^2} + \frac{\partial^2 \theta_u}{\partial Y^2}\right),\ \lambda_2(Fo_2) < X, Y < 1 \tag{41}$$

Initial and boundary condition are given as:

$$\theta_m(X, Y, Fo_1{}^*) = \theta_u(X, Y, Fo_1{}^*), \tag{42}$$

$$\frac{\partial \theta_m}{\partial X}(1, Y, Fo_1) = 0, \tag{43}$$

$$\frac{\partial \theta_m}{\partial Y}(X, 1, Fo_1) = 0, \tag{44}$$

$$\theta_m(\lambda_2(Fo_2), Fo_2) = \theta_u(\lambda_2(Fo_2), Fo_2) = 0 \tag{45}$$

Interface condition is given by:

$$\frac{\partial \theta_m}{\partial X} - k_{um}\frac{\partial \theta_u}{\partial X} = \frac{-1}{Ste_2}\frac{\partial X}{\partial Fo_2},\ X = \lambda_2(Fo_2) \tag{46}$$

where

$$\theta_m = \frac{T_l - T_m}{T_o - T_l},\ \theta_u = \frac{T_l - T_u}{T_o - T_l},\ Fo_1^* = Fo_2 - Fo_1,\ a_{12} = \frac{a_1}{a_2}.$$

Stage III

$$\frac{\partial \theta_f}{\partial Fo_3} = \frac{\partial^2 \theta_f}{\partial X^2} + \frac{\partial^2 \theta_f}{\partial Y^2},\ 0 < X, Y < \lambda_1(Fo_3) \tag{47}$$

$$\left(1 - \frac{1}{Ste_3}\right)\frac{\partial \theta_m}{\partial Fo_3} = a_{23}\left(\frac{\partial^2 \theta_m}{\partial X^2} + \frac{\partial^2 \theta_m}{\partial Y^2}\right),\ \lambda_1(Fo_3) < X, Y < \lambda_2(Fo_3) \tag{48}$$

$$\frac{\partial \theta_u}{\partial Fo_3} = a_{13}\left(\frac{\partial^2 \theta_u}{\partial X^2} + \frac{\partial^2 \theta_u}{\partial Y^2}\right),\ \lambda_2(Fo_3) < X, Y < 1 \tag{49}$$

Initial and boundary condition are given as:

$$\theta_f(X, Y, Fo_2{}^*) = \theta_m(X, Y, Fo_2{}^*) = \theta_u(X, Y, Fo_2{}^*), \tag{50}$$

$$\frac{\partial \theta_f}{\partial X}(1, Y, Fo_1) = 0, \tag{51}$$

$$\frac{\partial \theta_f}{\partial Y}(X, 1, Fo_1) = 0, \tag{52}$$

$$\theta_f(\lambda_1(Fo_3), Fo_3) = \theta_m(\lambda_1(Fo_3), Fo_3) = \theta_s, \tag{53}$$

$$\theta_m(\lambda_2(Fo_3), Fo_3) = \theta_u(\lambda_2(Fo_3), Fo_3) = 1 \tag{54}$$

Interface condition are given by:

$$\frac{\partial \theta_f}{\partial X} - k_{mf}\frac{\partial \theta_m}{\partial X} = \frac{-1}{Ste_3}\frac{\partial X}{\partial Fo_3},\ X = \lambda_1(Fo_3), \tag{55}$$

$$\frac{\partial \theta_m}{\partial X} - k_{um}\frac{\partial \theta_u}{\partial X} = \frac{-1}{Ste_3}\frac{\partial X}{\partial Fo_3},\ X = \lambda_2(Fo_3). \tag{56}$$

where

$$\theta_f = \frac{T_f - T_s}{T_l - T_s},\ \theta_m = \frac{T_m - T_s}{T_l - T_s},\ \theta_u = \frac{T_u - T_s}{T_l - T_s},$$
$$Fo_2^* = Fo_3 - Fo_2,\ a_{23} = \frac{a_2}{a_3},\ a_{13} = \frac{a_1}{a_3}.$$

2.1. Boundary condition in dimensionless form

Now also reducing boundary conditions in dimensionless form, Eqns. (11)–(13) becomes:

$$A_1\frac{\partial\theta}{\partial X}(0,\ Y,\ F_o) + B_1\theta(0,\ Y,\ F_o) = g(F_o) \tag{57}$$

I kind:

$$\theta(0,\ Y,\ F_o) = \theta_w \tag{58}$$

II kind:

$$\frac{\partial\theta}{\partial X}(0,\ Y,\ F_o) = -K_i \tag{59}$$

III kind:

$$\frac{\partial\theta}{\partial X}(0,\ Y,\ F_o) = -Bi(\theta_w - \theta_s). \tag{60}$$

3. Solution of the problem

Using finite differences and after simple algebraic computation, our problem reduces as follows:

Boundary condition of I kind:

For Stage I,

$$Fo_q\frac{d^2\Theta_u}{dFo_1^2} + (I + P_f^2Fo_q - Fo_TU_1)\frac{d\Theta_u}{dFo_1} + (P_f^2I - U_1)\Theta_u = (P_f^2\theta_b + P_m)d + \frac{\theta_w}{h^2}d_1 + \frac{\theta_r}{h^2}d_2 + \frac{\theta_r}{k^2}d_3 \tag{61}$$

where Θ_u, U_1, d, d_1, d_2 and d_3 are given by:

$$\Theta_u = \begin{pmatrix}\theta_u^1\\ \theta_u^2\\ \theta_u^3\\ \vdots\\ \vdots\\ \theta_u^N\end{pmatrix}_{N\times1},\quad U_1 = \frac{1}{(h^2+k^2)}\begin{pmatrix}-2,1,0,\ .....0,0,0\\ 1,\ -2,1,\ .....0,0,0\\ 0,1,\ -2,\ .....0,0,0\\ \vdots,...,\vdots;...;\vdots,...,\vdots\\ \vdots,...,\vdots;...;\vdots,...,\vdots\\ 0,0,0,\ .....,1,\ -2,0\\ 0,0,0,\ .....,0,2,\ -2\end{pmatrix}_{N\times N},$$

$$d = \begin{pmatrix}1\\1\\1\\\vdots\\\vdots\\1\end{pmatrix}_{N\times1},\ d_1 = \begin{pmatrix}1\\0\\0\\\vdots\\\vdots\\0\end{pmatrix}_{N\times1},\ d_2 = \begin{pmatrix}0\\0\\0\\\vdots\\\vdots\\1\end{pmatrix}_{N\times1},\ d_3 = \begin{pmatrix}1\\0\\0\\\vdots\\\vdots\\1\end{pmatrix}_{N\times1}.$$

For Stage II,

$$\left(1 + \frac{1}{Ste_2}\right)\frac{d\Theta_m}{dFo_2} - U_2\Theta_m = \frac{\theta_w}{h^2}d_1 + \frac{\theta_r}{h^2}d_2 + \frac{\theta_r}{k^2}d_3,\ 0 < X,\ Y < \lambda_2(Fo_2), \tag{62}$$

$$\frac{d\Theta_u}{dFo_2} - a_{12}U_3\Theta_u = 0,\ \lambda_2(Fo_2) < X,\ Y < 1 \tag{63}$$

$$\Theta_m(Fo_1^*) = \Theta_u(Fo_1^*) \tag{64}$$

where Θ_m, Θ_u, U_2 and U_3 are given as follows:

$$\Theta_m = \begin{pmatrix}\theta_m^1\\ \theta_m^2\\ \theta_m^3\\ \vdots\\ \vdots\\ \theta_m^{\bar N-1}\end{pmatrix}_{\bar N-1\times1},\quad U_2 = \frac{1}{(h^2+k^2)}\begin{pmatrix}-2,1,0,\ .....0,0,0\\ 1,\ -2,1,\ .....0,0,0\\ 0,1,\ -2,\ .....0,0,0\\ \vdots,...,\vdots;...;\vdots,...,\vdots\\ \vdots,...,\vdots;...;\vdots,...,\vdots\\ 0,0,0,\ .....,1,\ -2,0\\ 0,0,0,\ .....,0,1,\ -2\end{pmatrix}_{\bar N-1\times\bar N-1},$$

$$\Theta_u = \begin{pmatrix}\theta_u^{\bar N+1}\\ \theta_u^{\bar N+2}\\ \theta_u^{\bar N+3}\\ \vdots\\ \vdots\\ \theta_u^N\end{pmatrix}_{N-\bar N\times1},\quad U_3 = \frac{1}{(h^2+k^2)}\begin{pmatrix}-2,1,0,\ .....0,0,0\\ 1,\ -2,1,\ .....0,0,0\\ 0,1,\ -2,\ .....0,0,0\\ \vdots,...,\vdots;...;\vdots,...,\vdots\\ \vdots,...,\vdots;...;\vdots,...,\vdots\\ 0,0,0,\ .....,1,\ -2,0\\ 0,0,0,\ .....,0,2,\ -2\end{pmatrix}_{N-\bar N\times N-\bar N}$$

For Stage III,

$$\frac{d\Theta_f}{dFo_3} - U_4\Theta_f = \frac{\theta_s}{(h^2+k^2)}d' + \frac{\theta_w}{(h^2+k^2)}d_1',\ 0 < X,\ Y < \lambda_1(Fo_3) \tag{65}$$

$$\left(1 - \frac{1}{Ste_3}\right)\frac{d\Theta_m}{dFo_3} - a_{23}U_5\Theta_m = \frac{1}{(h^2+k^2)}d_2',\ \lambda_1(Fo_3) < X,\ Y < \lambda_2(Fo_3) \tag{66}$$

$$\frac{d\Theta_u}{dFo_3} - a_{13}U_6\Theta_u = \frac{1}{(h^2+k^2)}d_3',\ \lambda_2(Fo_3) < X,\ Y < 1 \tag{67}$$

$$\Theta_f(Fo_2^*) = \Theta_m(Fo_2^*) = \Theta_u(Fo_2^*) \tag{68}$$

where,

$$\Theta_f = \begin{pmatrix}\theta_f^1\\ \theta_f^2\\ \theta_f^3\\ \vdots\\ \vdots\\ \theta_f^{\bar p-1}\end{pmatrix}_{\bar p-1\times1},\quad U_4 = \frac{1}{(h^2+k^2)}\begin{pmatrix}-2,1,0,\ .....0,0,0\\ 1,\ -2,1,\ .....0,0,0\\ 0,1,\ -2,\ .....0,0,0\\ \vdots,...,\vdots;...;\vdots,...,\vdots\\ \vdots,...,\vdots;...;\vdots,...,\vdots\\ 0,0,0,\ .....,1,\ -2,0\\ 0,0,0,\ .....,0,1,\ -2\end{pmatrix}_{\bar p-1\times\bar p-1},$$

$$\Theta_m = \begin{pmatrix}\theta_m^1\\ \theta_m^2\\ \theta_m^3\\ \vdots\\ \vdots\\ \theta_m^{\bar q-1}\end{pmatrix}_{\bar q-1\times1},\quad U_5 = \frac{1}{(h^2+k^2)}\begin{pmatrix}-2,1,0,\ .....0,0,0\\ 1,\ -2,1,\ .....0,0,0\\ 0,1,\ -2,\ .....0,0,0\\ \vdots,...,\vdots;...;\vdots,...,\vdots\\ \vdots,...,\vdots;...;\vdots,...,\vdots\\ 0,0,0,\ .....,1,\ -2,0\\ 0,0,0,\ .....,0,1,\ -2\end{pmatrix}_{q\times q},$$

$$\Theta_u = \begin{pmatrix}\theta_u^1\\ \theta_u^2\\ \theta_u^3\\ \vdots\\ \vdots\\ \theta_u^{\bar r-1}\end{pmatrix}_{\bar r-1\times1},\quad U_6 = \frac{1}{(h^2+k^2)}\begin{pmatrix}-2,1,0,\ .....0,0,0\\ 1,\ -2,1,\ .....0,0,0\\ 0,1,\ -2,\ .....0,0,0\\ \vdots,...,\vdots;...;\vdots,...,\vdots\\ \vdots,...,\vdots;...;\vdots,...,\vdots\\ 0,0,0,\ .....,1,\ -2,0\\ 0,0,0,\ .....,0,2,\ -2\end{pmatrix}_{r\times r} \tag{69}$$

$$d' = \begin{pmatrix}1\\1\\1\\\vdots\\\vdots\\1\end{pmatrix}_{p\times1},\ d_1' = \begin{pmatrix}1\\0\\0\\\vdots\\\vdots\\0\end{pmatrix}_{p\times1},\ d_2' = \begin{pmatrix}0\\0\\0\\\vdots\\\vdots\\1\end{pmatrix}_{q\times1},\ d_3' = \begin{pmatrix}1\\0\\0\\\vdots\\\vdots\\0\end{pmatrix}_{r\times1}.$$

Boundary condition of II kind:

For Stage I,

$$Fo_q\frac{d^2\Theta_u}{dFo_1^2} + (1 + P_f^2Fo_q - Fo_TU_1')\frac{d\Theta_u}{dFo_1} + (P_f^2I - U_1')\Theta_u = (P_f^2\theta_b + P_m)d + \frac{K_i}{h}d_1 - \frac{K_i}{h}d_2 + \frac{K_i}{k}d_1 - \frac{K_i}{k}d_2 \tag{70}$$

where Θ_u and U_1' are given by:

$$\Theta_u = \begin{pmatrix}\theta_u^1\\ \theta_u^2\\ \theta_u^3\\ \vdots\\ \vdots\\ \theta_u^N\end{pmatrix}_{N\times1},\quad U_1' = \frac{1}{(h^2+k^2)}\begin{pmatrix}-1,1,0,\ .....0,0,0\\ 1,\ -1,1,\ .....0,0,0\\ 0,1,\ -1,\ .....0,0,0\\ \vdots,...,\vdots;...;\vdots,...,\vdots\\ \vdots,...,\vdots;...;\vdots,...,\vdots\\ 0,0,0,\ .....,1,\ -1,0\\ 0,0,0,\ .....,0,2,\ -1\end{pmatrix}_{N\times N},$$

For Stage II,

$$\left(1 + \frac{1}{Ste_2}\right)\frac{d\Theta_m}{dFo_2} - U_2'\Theta_m = \frac{K_i}{h}d_1 - \frac{K_i}{h}d_2 + \frac{K_i}{k}d_1 - \frac{K_i}{k}d_2,\ 0 < X,\ Y < \lambda_2(Fo_2), \tag{71}$$

$$\frac{d\Theta_u}{dFo_2} - a_{12}U_3'\Theta_u = 0,\ \lambda_2(Fo_2) < X,\ Y < 1 \tag{72}$$

$$\Theta_m(Fo_1^*) = \Theta_u(Fo_1^*) \tag{73}$$

where Θ_m, Θ_u, U_2' and U_3' are given as follows:

$$\Theta_m = \begin{pmatrix} \theta_m^1 \\ \theta_m^2 \\ \theta_m^3 \\ \vdots \\ \vdots \\ \theta_m^{\tilde{N}-1} \end{pmatrix}_{\tilde{N}-1\times 1}, \quad U_2' = \frac{1}{(h^2+k^2)} \begin{pmatrix} -1,1,0, \ldots\ldots 0,0,0 \\ 1,-1,1, \ldots\ldots 0,0,0 \\ 0,1,-1, \ldots\ldots 0,0,0 \\ \vdots,\ldots,\vdots;\ldots;\vdots,\ldots,\vdots \\ \vdots,\ldots,\vdots;\ldots;\vdots,\ldots,\vdots \\ 0,0,0, \ldots\ldots,1,-1,0 \\ 0,0,0, \ldots\ldots,0,1,-1 \end{pmatrix}_{\tilde{N}-1\times\tilde{N}-1},$$

$$\Theta_u = \begin{pmatrix} \theta_u^{\tilde{N}+1} \\ \theta_u^{\tilde{N}+2} \\ \theta_u^{\tilde{N}+3} \\ \vdots \\ \vdots \\ \theta_u^{N} \end{pmatrix}_{N-\tilde{N}\times 1}, \quad U_3' = \frac{1}{(h^2+k^2)} \begin{pmatrix} -1,1,0, \ldots\ldots 0,0,0 \\ 1,-1,1, \ldots\ldots 0,0,0 \\ 0,1,-1, \ldots\ldots 0,0,0 \\ \vdots,\ldots,\vdots;\ldots;\vdots,\ldots,\vdots \\ \vdots,\ldots,\vdots;\ldots;\vdots,\ldots,\vdots \\ 0,0,0, \ldots\ldots,1,-1,0 \\ 0,0,0, \ldots\ldots,0,2,-1 \end{pmatrix}_{N-\tilde{N}\times N-\tilde{N}}$$

For Stage III,

$$\frac{d\Theta_f}{dFo_3} - U_4'\Theta_f = \frac{K_i}{h}d_1 - \frac{K_i}{h}d_2 + \frac{K_i}{k}d_1 - \frac{K_i}{k}d_2,\ 0 < X, Y < \lambda_1(Fo_3) \tag{74}$$

$$\left(1 - \frac{1}{Ste_3}\right)\frac{d\Theta_m}{dFo_3} - a_{23}U_5'\Theta_m = \frac{1}{(h^2+k^2)}d_3',\ \lambda_1(Fo_3) < X, Y < \lambda_2(Fo_3) \tag{75}$$

$$\frac{d\Theta_u}{dFo_3} - a_{13}U_6'\Theta_u = \frac{1}{(h^2+k^2)}d_3',\ \lambda_2(Fo_3) < X, Y < 1 \tag{76}$$

$$\Theta_m(Fo_2^*) = \Theta_u(Fo_2^*) = \Theta_f(Fo_2^*) \tag{77}$$

where,

$$\Theta_f = \begin{pmatrix} \theta_f^1 \\ \theta_f^2 \\ \theta_f^3 \\ \vdots \\ \theta_f^{\bar{p}-1} \end{pmatrix}_{\bar{p}-1\times 1}, \quad U_4' = \frac{1}{(h^2+k^2)} \begin{pmatrix} -1,1,0, \ldots\ldots 0,0,0 \\ 1,-1,1, \ldots\ldots 0,0,0 \\ 0,1,-1, \ldots\ldots 0,0,0 \\ \vdots,\ldots,\vdots;\ldots;\vdots,\ldots,\vdots \\ \vdots,\ldots,\vdots;\ldots;\vdots,\ldots,\vdots \\ 0,0,0, \ldots\ldots,1,-1,0 \\ 0,0,0, \ldots\ldots,0,1,-1 \end{pmatrix}_{\bar{p}-1\times\bar{p}-1}, \tag{78}$$

$$\Theta_m = \begin{pmatrix} \theta_m^1 \\ \theta_m^2 \\ \theta_m^3 \\ \vdots \\ \theta_m^{\bar{q}-1} \end{pmatrix}_{\bar{q}-1\times 1}, \quad U_5' = \frac{1}{(h^2+k^2)} \begin{pmatrix} -1,1,0, \ldots\ldots 0,0,0 \\ 1,-1,1, \ldots\ldots 0,0,0 \\ 0,1,-1, \ldots\ldots 0,0,0 \\ \vdots,\ldots,\vdots;\ldots;\vdots,\ldots,\vdots \\ \vdots,\ldots,\vdots;\ldots;\vdots,\ldots,\vdots \\ 0,0,0, \ldots\ldots,1,-1,0 \\ 0,0,0, \ldots\ldots,0,1,-1 \end{pmatrix}_{q\times q},$$

$$\Theta_u = \begin{pmatrix} \theta_u^1 \\ \theta_u^2 \\ \theta_u^3 \\ \vdots \\ \theta_u^{\bar{r}-1} \end{pmatrix}_{\bar{r}-1\times 1}, \quad U_6' = \frac{1}{(h^2+k^2)} \begin{pmatrix} -1,1,0, \ldots\ldots 0,0,0 \\ 1,-1,1, \ldots\ldots 0,0,0 \\ 0,1,-1, \ldots\ldots 0,0,0 \\ \vdots,\ldots,\vdots;\ldots;\vdots,\ldots,\vdots \\ \vdots,\ldots,\vdots;\ldots;\vdots,\ldots,\vdots \\ 0,0,0, \ldots\ldots,1,-1,0 \\ 0,0,0, \ldots\ldots,0,2,-1 \end{pmatrix}_{r\times r}$$

Boundary condition of III kind:
For Stage I,

$$Fo_q\frac{d^2\Theta_u}{dFo_1^2} + (1 + P_f^2Fo_q - Fo_T U_1'')\frac{d\Theta_u}{dFo_1} + (P_f^2 I - U_1'')\Theta_u = (P_f^2\theta_b + P_m)d + \frac{Bi(\theta_w-\theta_r)}{h}d_1 - \frac{Bi(\theta_w-\theta_r)}{h}d_2 + \frac{Bi(\theta_w-\theta_r)}{k}d_1 - \frac{Bi(\theta_w-\theta_r)}{k}d_2 \tag{79}$$

where Θ_u and U_1'' are given by:

$$\Theta_u = \begin{pmatrix} \theta_u^1 \\ \theta_u^2 \\ \theta_u^3 \\ \vdots \\ \theta_u^N \end{pmatrix}_{N\times 1}, \quad U_1'' = \frac{1}{(h^2+k^2)} \begin{pmatrix} -1,1,0, \ldots\ldots 0,0,0 \\ 1,-1,1, \ldots\ldots 0,0,0 \\ 0,1,-1, \ldots\ldots 0,0,0 \\ \vdots,\ldots,\vdots;\ldots;\vdots,\ldots,\vdots \\ \vdots,\ldots,\vdots;\ldots;\vdots,\ldots,\vdots \\ 0,0,0, \ldots\ldots,1,-1,0 \\ 0,0,0, \ldots\ldots,0,2,-1 \end{pmatrix}_{N\times N},$$

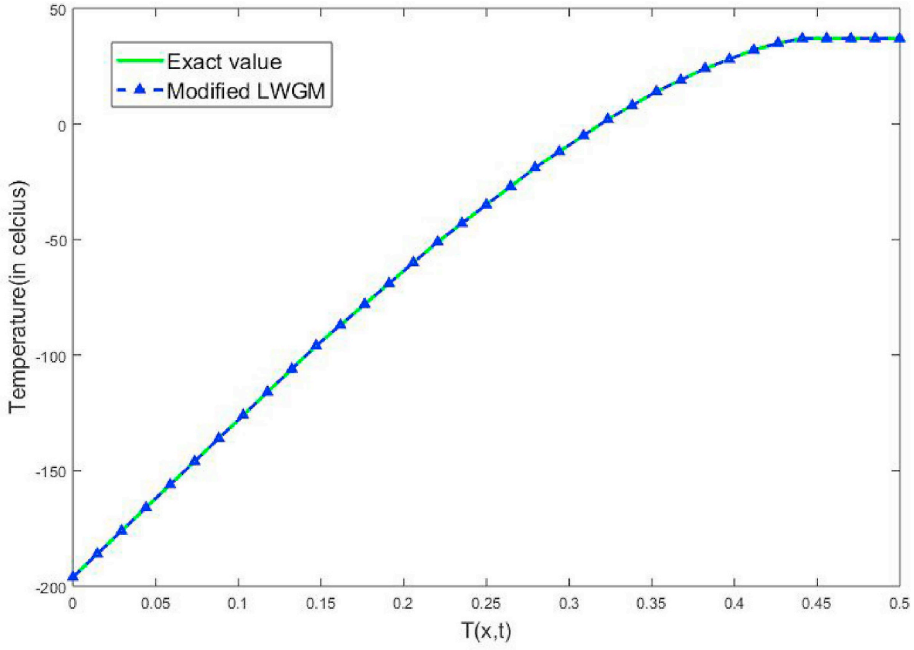

Fig. 2. Temperature distribution T(x,t) for one-dimensional at time t = 900 s calculated using physical properties(Table 1); $T_0 = 37^0C$, $T_c = -196^0C$; length = 0.5m.

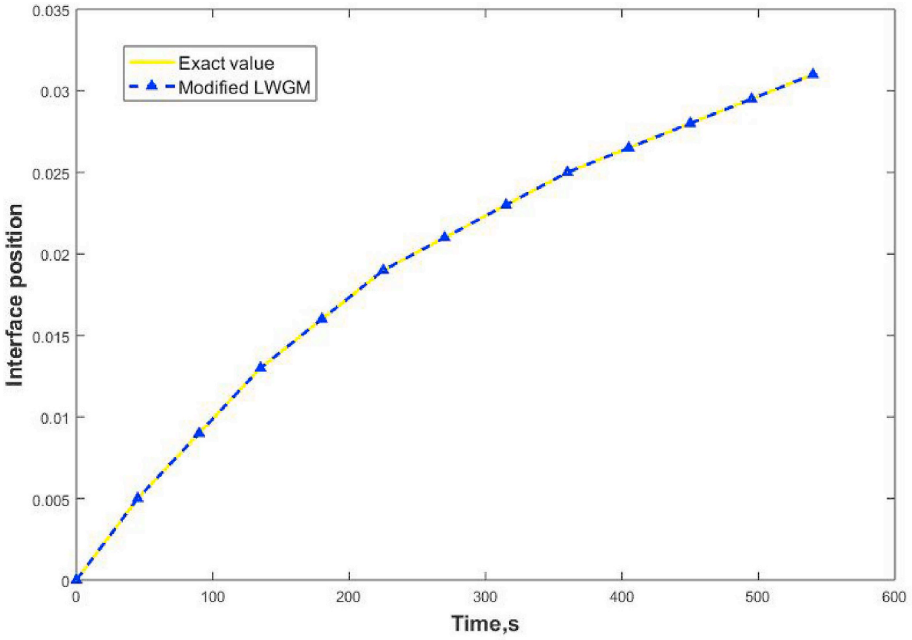

Fig. 3. Interface position for one-dimensional case considering the time calculated using physical properties(Table 1); $T_0 = 37^0C$, $T_c = -196^0C$; length = 0.5m.

Table 1
Thermal-physical properties of tissues(Bischof et al.).

Parameter	unit of measurement	value
Density of unfrozen lung tissue	kg/m^3	161
Density of frozen lung tissue	kg/m^3	149
Density of unfrozen tumor tissue	kg/m^3	998
Density of frozen tumor tissue	kg/m^3	921
Density of blood	kg/m^3	1005
Thermal conductivity of unfrozen lung tissue	W/m^0C	0.11
Thermal conductivity of frozen lung tissue	W/m^0C	0.38
Thermal conductivity of unfrozen tumor tissue	W/m^0C	0.552
Thermal conductivity of frozen tumor tissue	W/m^0C	2.25
Specific heat of unfrozen lung tissue	J/kg^0C	4174
Specific heat of frozen lung tissue	J/kg^0C	1221
Specific heat of unfrozen tumor tissue	J/kg^0C	4200
Specific heat of frozen tumor tissue	J/kg^0C	1230
Blood perfusion in lung tissue	ml/sl	0.0005
Blood perfusion in tumor tissue	ml/sl	0.002
Metabolic heat generation in lung	W/m^3	42,000
Metabolic heat generation in tumor	W/m^3	672
Latent heat	kJ/kg	333
Arterial blood temperature	$^{\circ}C$	37

For Stage II,

$$\left(1+\frac{1}{Ste_2}\right)\frac{d\Theta_m}{dFo_2} - U_2''\Theta_m = \frac{B_i(\theta_w-\theta_r)}{h}d_1 - \frac{B_i(\theta_w-\theta_r)}{h}d_2 + \frac{B_i(\theta_w-\theta_r)}{k}d_1 - \frac{B_i(\theta_w-\theta_r)}{k}d_2,\ 0<X,\ Y<\lambda_2(Fo_2), \tag{80}$$

$$\frac{d\Theta_u}{dFo_2} - a_{12}U_3''\Theta_u = 0,\ \lambda_2(Fo_2)<X,\ Y<1 \tag{81}$$

$$\Theta_m(Fo_1^*) = \Theta_u(Fo_1^*) \tag{82}$$

where Θ_m, Θ_u, U_2'' and U_3'' are given as follows:

$$\Theta_m = \begin{pmatrix} \theta_m^1 \\ \theta_m^2 \\ \theta_m^3 \\ \vdots \\ \vdots \\ \theta_m^{\tilde{N}-1} \end{pmatrix}_{\tilde{N}-1\times 1},\quad U_2'' = \frac{1}{(h^2+k^2)}\begin{pmatrix} -1,1,0,\ .....0,0,0 \\ 1,\ -1,1,\ .....0,0,0 \\ 0,1,\ -1,\ .....0,0,0 \\ \vdots,...,\vdots;...;\vdots,...,\vdots \\ \vdots,...,\vdots;...;\vdots,...,\vdots \\ 0,0,0,\ .....,1,\ -1,0 \\ 0,0,0,\ .....,0,1,\ -1 \end{pmatrix}_{\tilde{N}-1\times\tilde{N}-1},$$

$$\Theta_u = \begin{pmatrix} \theta_u^{\tilde{N}+1} \\ \theta_u^{\tilde{N}+2} \\ \theta_u^{\tilde{N}+3} \\ \vdots \\ \vdots \\ \theta_u^{N} \end{pmatrix}_{N-\tilde{N}\times 1},\quad U_3'' = \frac{1}{(h^2+k^2)}\begin{pmatrix} -1,1,0,\ .....0,0,0 \\ 1,\ -1,1,\ .....0,0,0 \\ 0,1,\ -1,\ .....0,0,0 \\ \vdots,...,\vdots;...;\vdots,...,\vdots \\ \vdots,...,\vdots;...;\vdots,...,\vdots \\ 0,0,0,\ .....,1,\ -1,0 \\ 0,0,0,\ .....,0,2,\ -1 \end{pmatrix}_{N-\tilde{N}\times N-\tilde{N}},$$

For Stage III,

$$\frac{d\Theta_f}{dFo_3} - U_4''\Theta_f = \frac{B_i(\theta_w-\theta_r)}{h}d_1 - \frac{B_i(\theta_w-\theta_r)}{h}d_2 + \frac{B_i(\theta_w-\theta_r)}{k}d_1 - \frac{B_i(\theta_w-\theta_r)}{k}d_2,\ 0<X,\ Y<\lambda_1(Fo_3) \tag{83}$$

$$\left(1-\frac{1}{Ste_3}\right)\frac{d\Theta_m}{dFo_3} - a_{23}U_5'\Theta_m = \frac{1}{(h^2+k^2)}d_2',\ \lambda_1(Fo_3)<X,\ Y<\lambda_2(Fo_3) \tag{84}$$

$$\frac{d\Theta_u}{dFo_3} - a_{13}U_6'\Theta_u = \frac{1}{(h^2+k^2)}d_3',\ \lambda_2(Fo_3)<X,\ Y<1 \tag{85}$$

$$\Theta_m(Fo_2^*) = \Theta_u(Fo_2^*) = \Theta_f(Fo_2^*) \tag{86}$$

where,

$$\Theta_f = \begin{pmatrix} \theta_f^1 \\ \theta_f^2 \\ \theta_f^3 \\ \vdots \\ \vdots \\ \theta_f^{\bar{p}-1} \end{pmatrix}_{\bar{p}-1\times 1}, \quad U_4' = \frac{1}{(h^2+k^2)} \begin{pmatrix} -1,1,0, \ldots\ldots.0,0,0 \\ 1, -1,1, \ldots\ldots.0,0,0 \\ 0,1, -1, \ldots\ldots.0,0,0 \\ \vdots,\ldots,\vdots;\ldots;\vdots,\ldots,\vdots \\ \vdots,\ldots,\vdots;\ldots;\vdots,\ldots,\vdots \\ 0,0,0, \ldots\ldots.,1, -1,0 \\ 0,0,0, \ldots\ldots.,0,1, -1 \end{pmatrix}_{\bar{p}-1\times\bar{p}-1},$$

$$\Theta_m = \begin{pmatrix} \theta_m^1 \\ \theta_m^2 \\ \theta_m^3 \\ \vdots \\ \vdots \\ \theta_m^{\bar{q}-1} \end{pmatrix}_{\bar{q}-1\times 1}, \quad U_5' = \frac{1}{(h^2+k^2)} \begin{pmatrix} -1,1,0, \ldots\ldots.0,0,0 \\ 1, -1,1, \ldots\ldots.0,0,0 \\ 0,1, -1, \ldots\ldots.0,0,0 \\ \vdots,\ldots,\vdots;\ldots;\vdots,\ldots,\vdots \\ \vdots,\ldots,\vdots;\ldots;\vdots,\ldots,\vdots \\ 0,0,0, \ldots\ldots.,1, -1,0 \\ 0,0,0, \ldots\ldots.,0,1, -1 \end{pmatrix}_{q\times q},$$

$$\Theta_u = \begin{pmatrix} \theta_u^1 \\ \theta_u^2 \\ \theta_u^3 \\ \vdots \\ \vdots \\ \theta_u^{\bar{r}-1} \end{pmatrix}_{\bar{r}-1\times 1}, \quad U_6' = \frac{1}{(h^2+k^2)} \begin{pmatrix} -1,1,0, \ldots\ldots.0,0,0 \\ 1, -1,1, \ldots\ldots.0,0,0 \\ 0,1, -1, \ldots\ldots.0,0,0 \\ \vdots,\ldots,\vdots;\ldots;\vdots,\ldots,\vdots \\ \vdots,\ldots,\vdots;\ldots;\vdots,\ldots,\vdots \\ 0,0,0, \ldots\ldots.,1, -1,0 \\ 0,0,0, \ldots\ldots.,0,2, -1 \end{pmatrix}_{r\times r}.$$

4. Modified Legendre wavelet Galerkin Method

We are using Legendre wavelet Galerkin method to solve our problem in all the stages with generalized boundary condition are as follows:

Boundary condition of I kind

4.1. Stage 1

Let us assume that the unknown function $\frac{d^2\Theta_u}{dFo_1^2}$ is approximated by

$$\frac{d^2\Theta_u}{dFo_1^2} \cong C\bar{\psi}(Fo_1), \tag{87}$$

where C is unknown matrix of order $N \times 2^{2(k-1)}M^2$ and $\bar{\psi}(Fo_1)$ is a matrix of order $2^{2(k-1)}M^2 \times J$ defined by

$$\bar{\psi} = \begin{pmatrix} \psi & 0 & \cdots & 0 \\ 0 & \psi & \cdots & 0 \\ \vdots & \vdots & \ddots & \vdots \\ 0 & 0 & \cdots & \psi \end{pmatrix}$$

where$\psi(Fo) = [\psi_{1,0},\ \psi_{1,1},\ \ldots,\ \psi_{1,M-1},\ \ldots,\ \psi_{2^{k-1},0},\ \psi_{2^{k-1},1},\ \ldots\ \psi_{2^{k-1},M-1}]'$ and the elements of $\psi(Fo)$ is defined by

$$\psi_{n,m}(Fo_1) = \begin{cases} \sqrt{(m+1/2)}\,2^{k/2}P_m(2^kFo_1 - \hat{n}), & \frac{\hat{n}-1}{2^k} \le Fo_1 \le \frac{\hat{n}+1}{2^k} \\ 0 & , otherwise. \end{cases}$$

where $k = 1,2,3\ldots$, $n = 1,2,\ \ldots,2^{k-1}$, $\hat{n} = 2n-1$ and m is the order of Legendre polynomial (Yadav et al., 2014). $P_m(Fo_1)$ is denoted by Legendre polynomial of order m, $m = 0,1,\ \ldots,M-1$, which are orthogonal with respect to the weight function $w(Fo_1) = 1$ on the interval $[-1,1]$, and satisfy the following recursive formula

$$P_0(Fo_1) = 1,$$
$$P_1(Fo_1) = Fo_1,$$
$$P_{m+1}(Fo_1) = \frac{2m+1}{m+1}Fo_1P_m(Fo_1) - \frac{m}{m+1}P_{m-1}(Fo_1).$$

The operational matrix of integration of ψ defined in (Kumar et al., 2016, 2018; Razzaghi and Yousefi, 2001) and given by

$$\int_0^{Fo_1} \psi(t)dt = P\psi(Fo_1) \tag{88}$$

where P if is the operational matrix of integration of order $2^{k-1}M \times 1$, given by

$$P = \frac{1}{2^k}\begin{pmatrix} L & O & O & \cdots & O \\ 0 & L & O & \cdots & O \\ 0 & 0 & L & \cdots & O \\ \vdots & \vdots & \vdots & \ddots & \vdots \\ 0 & 0 & 0 & \cdots & O \\ 0 & 0 & 0 & \cdots & O \end{pmatrix}$$

where O and L are $M \times M$ matrices given by $O = \begin{pmatrix} 2 & 0 & \cdots & 0 \\ 0 & 0 & \cdots & 0 \\ \vdots & \vdots & \ddots & \vdots \\ 0 & 0 & \cdots & 0 \end{pmatrix}$,

$$L = \begin{pmatrix} 1 & \frac{1}{\sqrt{3}} & 0 & 0 & \cdots & 0 & 0 & 0 \\ \frac{-1}{\sqrt{3}} & 0 & \frac{1}{\sqrt{15}} & 0 & \cdots & 0 & 0 & 0 \\ 0 & \frac{-1}{\sqrt{15}} & 0 & \frac{1}{\sqrt{35}} & \cdots & 0 & 0 & 0 \\ 0 & 0 & \frac{-1}{\sqrt{35}} & 0 & \cdots & 0 & 0 & 0 \\ \vdots & \vdots & \vdots & \vdots & \ddots & \vdots & \vdots & \vdots \\ 0 & 0 & 0 & 0 & \cdots & \frac{1}{\sqrt{(2M-3)(2M-5)}} & 0 & \frac{1}{\sqrt{(2M-3)(2M-1)}} \\ 0 & 0 & 0 & 0 & \cdots & 0 & \frac{-1}{\sqrt{(2M-1)(2M-3)}} & 0 \end{pmatrix}$$

respectively. Integrating (85) over 0 to Fo_1, we obtained

$$\frac{d\Theta_u}{dFo_1} \cong \frac{d\Theta_u}{dFo_1}(0) + \bar{P}\psi(Fo_1)$$
$$\frac{d\Theta_u}{dFo_1} \cong C\bar{P}\psi(Fo_1) \tag{89}$$

where $\bar{P}$ is defined as

$$\bar{P} = \begin{pmatrix} P & 0 & \cdots & 0 \\ 0 & P & \cdots & 0 \\ \vdots & \vdots & \ddots & \vdots \\ 0 & 0 & \cdots & P \end{pmatrix}$$

also

$$\int_0^{Fo} \bar{\psi}(Fo)dFo = \bar{P}\bar{\psi}(Fo)$$

Integrating again (85) over 0 to Fo_1, we obtained

$$\Theta_u \cong \Theta_u(0) + C\bar{P}^2\bar{\psi}(Fo_1)$$
$$\Theta_u \cong C\bar{P}^2\bar{\psi}(Fo_1) \tag{90}$$

After solving Eqns ((61), (85), (87) and (88), we obtained

$$Fo_qC\bar{\psi} + (I + P_f^2Fo_qI - Fo_TU)C\bar{P}\bar{\psi} + (P_f^2I - U)C\bar{P}^2\bar{\psi}$$
$$= (P_f^2\theta_b + P_m)H\bar{\psi} + \frac{\theta_w}{h^2}H_1\bar{\psi} + \frac{\theta_r}{h^2}H_2\bar{\psi} + \frac{\theta_r}{k^2}H_3\bar{\psi} \tag{91}$$

where $d = H\bar{\psi}$, $d1 = H_1\bar{\psi}$, $d2 = H_2\bar{\psi}$, $d3 = H_3\bar{\psi}$ and $Fod = F\bar{\psi}$

$$Fo_qC + (I + P_f^2Fo_qI - Fo_TU)C\bar{P} + (P_f^2I - U)C\bar{P}^2$$
$$= (P_f^2\theta_b + P_m)H + \frac{\theta_w}{h^2}H_1 + \frac{\theta_r}{h^2}H_2 + \frac{\theta_r}{k^2}H_3 \tag{92}$$

4.2. Stage 2

Let us assume that the unknown functions $\frac{d\Theta_m}{dFo_2}$ and $\frac{d\Theta_u}{dFo_2}$ are approximated by

$$\frac{d\Theta_m}{dFo_2} \cong D_1\bar{\psi}, \tag{93}$$

$$\frac{d\Theta_u}{dFo_2} \cong D_2\bar{\psi}, \tag{94}$$

Integrating (73,74) over Fo_1^* to Fo_2, we obtained

$$\Theta_m \cong D_1\bar{P}\bar{\psi} - D_1\bar{P}\bar{\psi}(Fo_1*), \tag{95}$$

$$\Theta_u \cong D_2\bar{P}\bar{\psi} - D_2\bar{P}\bar{\psi}(Fo_1*) \tag{96}$$

After solving Eqns (62), (91) and (93), we obtained

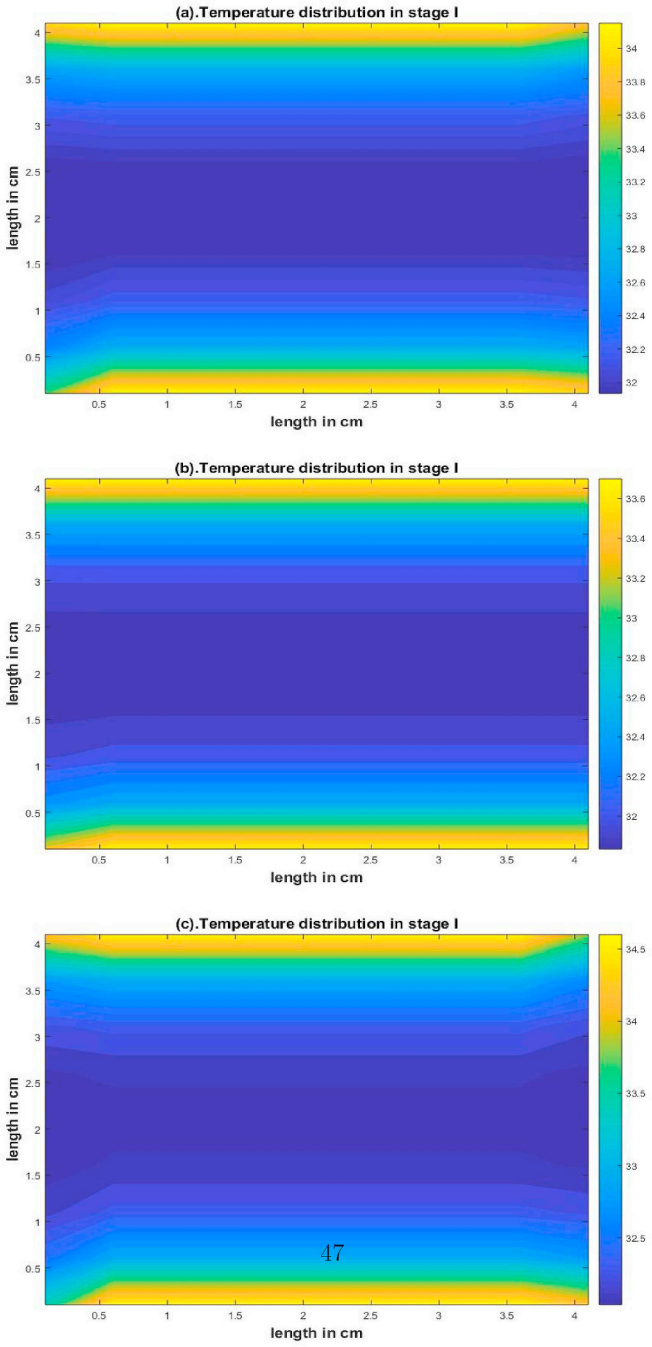

Fig. 4. Temperature distribution of unfrozen region in Stage1 at 200 s (a) I kind (b) II kind (c) III kind.

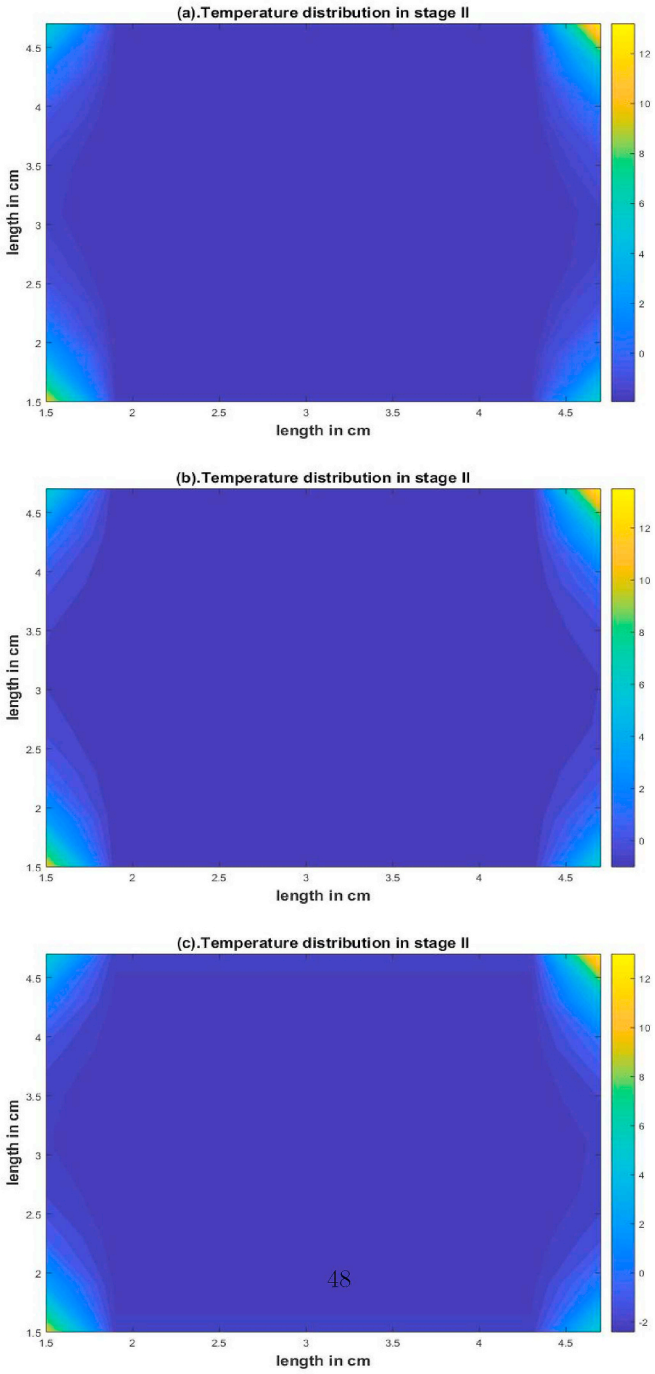

Fig. 5. Temperature distribution of unfrozen region in Stage1 at 200 s (a) I kind (b) II kind (c) III kind.

$$\left(1+\frac{1}{Ste_2}\right)D_1 I + D_1U_2\bar{P}\bar{\psi}(Fo_1{}^*)F - D_1U_2\bar{P} = \frac{\theta_w}{h^2}H_1 + \frac{\theta_r}{h^2}H_2 + \frac{\theta_r}{k^2}H_3 + U_2d_1F \tag{97}$$

After solving Eqns (63), (92) and (94), we obtained

$$D_2 I + a_{12}D_2U_3\bar{P}\bar{\psi}(Fo_1{}^*)F - a_{12}D_2U_3\bar{P} = \frac{1}{(h^2+k^2)}dF \tag{98}$$

4.3. Stage 3

Let us assume that the unknown functions $\frac{d\Theta_f}{dFo_3}$, $\frac{d\Theta_m}{dFo_3}$ and $\frac{d\Theta_u}{dFo_3}$ are approximated by

$$\frac{d\Theta_f}{dFo_3} \cong E_1\bar{\psi}, \tag{99}$$

$$\frac{d\Theta_m}{dFo_3} \cong E_2\bar{\psi}, \tag{100}$$

$$\frac{d\Theta_u}{dFo_3} \cong E_3\bar{\psi}, \tag{101}$$

Integrating (97–99) over Fo_2^* to Fo_3, we obtained

$$\Theta_f \cong E_1\bar{P}\psi - E_1\bar{P}\bar{\psi}(Fo_2^*), \tag{102}$$

$$\Theta_m \cong E_2\bar{P}\psi - E_2\bar{P}\bar{\psi}(Fo_2^*), \tag{103}$$

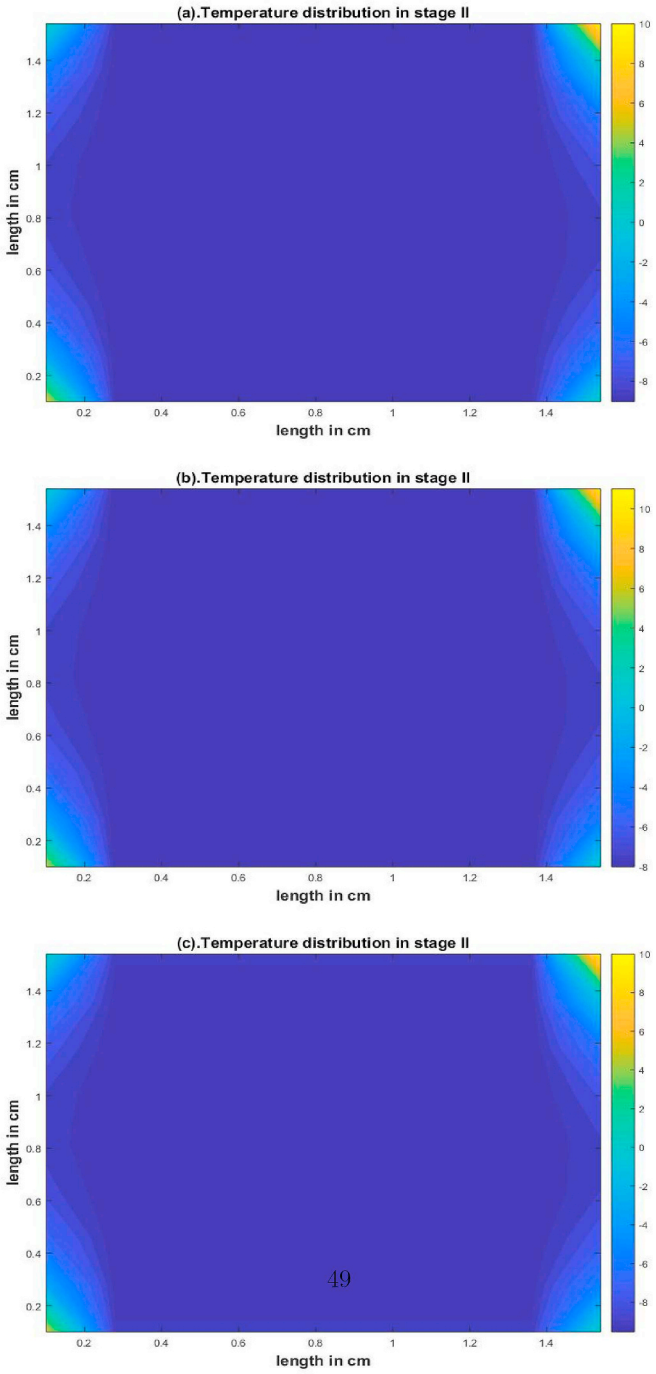

Fig. 6. Temperature distribution of mushy region in Stage2 at 500 s (a) I kind (b) II kind (c) III kind.

$$\Theta_u \cong E_3\bar{P}\psi - E_3\bar{P}\bar{\psi}(Fo_2^*). \tag{104}$$

After solving Eqns (65), (97) and (100), we obtained

$$E_1I + E_1U_4\bar{P}\bar{\psi}(Fo_2^*)F - E_1U_4\bar{P} = \frac{\theta_s}{(h^2+k^2)}H' + \frac{\theta_w}{(h^2+k^2)}H_1' \tag{105}$$

After solving Eqns (66), (98) and (101), we obtained

$$\left(1 - \frac{1}{Ste_3}\right)E_2I + a_{23}E_2U_5\bar{P}\bar{\psi}(Fo_2^*)F - a_{23}E_2U_5\bar{P} = \frac{\theta_w}{(h^2+k^2)}H_2' \tag{106}$$

After solving Eqns (67), (99) and (102), we obtained

$$E_3I + a_{13}E_3U_6\bar{P}\bar{\psi}(Fo_2^*)F - a_{13}E_3U_6\bar{P} = \frac{\theta_w}{(h^2+k^2)}H_3' \tag{107}$$

Boundary condition of II kind

4.4. Stage 1

After solving Eqns ((69), (85), (87) and (88), we obtained

$$Fo_qC + (I + P_f^2Fo_qI - Fo_TU')C\bar{P} + (P_f^2I - U')C\bar{P}^2 = (P_f^2\theta_b + P_m)H + \frac{K_i}{h}H_1 - \frac{K_i}{h}H_2 + \frac{K_i}{k}H_1 - \frac{K_i}{k}H_2 \tag{108}$$

4.5. Stage 2

After solving Eqns (70), (91) and (93), we obtained

$$\left(1 + \frac{1}{Ste_2}\right)D_1I + D_1U_2'\bar{P}\bar{\psi}(Fo_1{}^*)F - D_1U_2'\bar{P} = \frac{K_i}{h}H_1 - \frac{K_i}{h}H_2 + \frac{K_i}{k}H_1 - \frac{K_i}{k}H_2 \tag{109}$$

After solving Eqns (71), (92) and (94), we obtained

$$D_2I + a_{12}D_2U_3'\bar{P}\bar{\psi}(Fo_1{}^*)F - a_{12}D_2U_3'\bar{P} = \frac{1}{(h^2+k^2)}dF \tag{110}$$

4.6. Stage 3

After solving Eqns (73), (97) and (100), we obtained

$$E_1I + E_1U_4'\bar{P}\bar{\psi}(Fo_2^*)F - E_1U_4'\bar{P} = \frac{K_i}{h}H_1 - \frac{K_i}{h}H_2 + \frac{K_i}{k}H_1 - \frac{K_i}{k}H_2 \tag{111}$$

After solving Eqns (74), (98) and (101), we obtained

$$\left(1 - \frac{1}{Ste_3}\right)E_2I + a_{23}E_2U_5'\bar{P}\bar{\psi}(Fo_2^*)F - a_{23}E_2U_5'\bar{P} = \frac{1}{(h^2+k^2)}H_2' \tag{112}$$

After solving Eqns (75), (99) and (102), we obtained

$$E_3I + a_{13}E_3U_6'\bar{P}\bar{\psi}(Fo_2^*)F - a_{13}E_3U_6'\bar{P} = \frac{1}{(h^2+k^2)}H_3' \tag{113}$$

Boundary condition of III kind

4.7. Stage 1

After solving Eqns ((77), (85), (87) and (88), we obtained

$$Fo_qC + (I + P_f^2Fo_qI - Fo_TU_1'')C\bar{P} + (P_f^2I - U_1'')C\bar{P}^2 = (P_f^2\theta_b + P_m)H + \frac{B_i(\theta_w-\theta_r)}{h}H_1 - \frac{B_i(\theta_w-\theta_r)}{h}H_2 + \frac{B_i(\theta_w-\theta_r)}{k}H_1 - \frac{B_i(\theta_w-\theta_r)}{k}H_2 \tag{114}$$

4.8. Stage 2

After solving Eqns (78), (91) and (93), we obtained

$$\left(1 + \frac{1}{Ste_2}\right)D_1I + D_1U_2''\bar{P}\bar{\psi}(Fo_1{}^*)F - D_1U_2''\bar{P} = \frac{B_i(\theta_w-\theta_r)}{h}H_1 - \frac{B_i(\theta_w-\theta_r)}{h}H_2 + \frac{B_i(\theta_w-\theta_r)}{k}H_1 - \frac{B_i(\theta_w-\theta_r)}{k}H_2 \tag{115}$$

After solving Eqns (79), (92) and (94), we obtained

$$D_2I + a_{12}D_2U_3''\bar{P}\bar{\psi}(Fo_1{}^*)F - a_{12}D_2U_3''\bar{P} = \frac{1}{(h^2+k^2)}dF \tag{116}$$

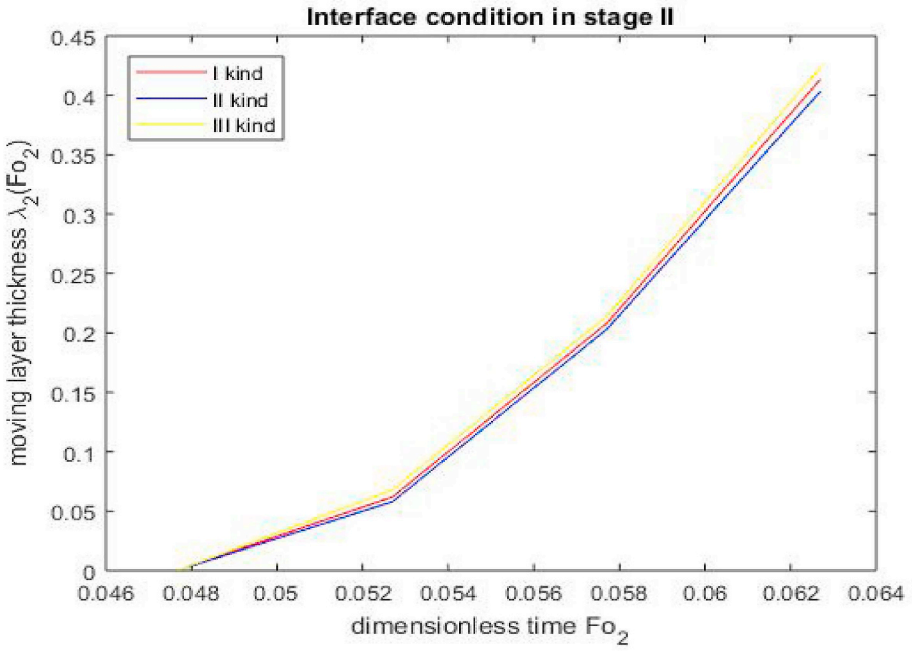

Fig. 7. Moving layer thickness λ_2 in stage2.

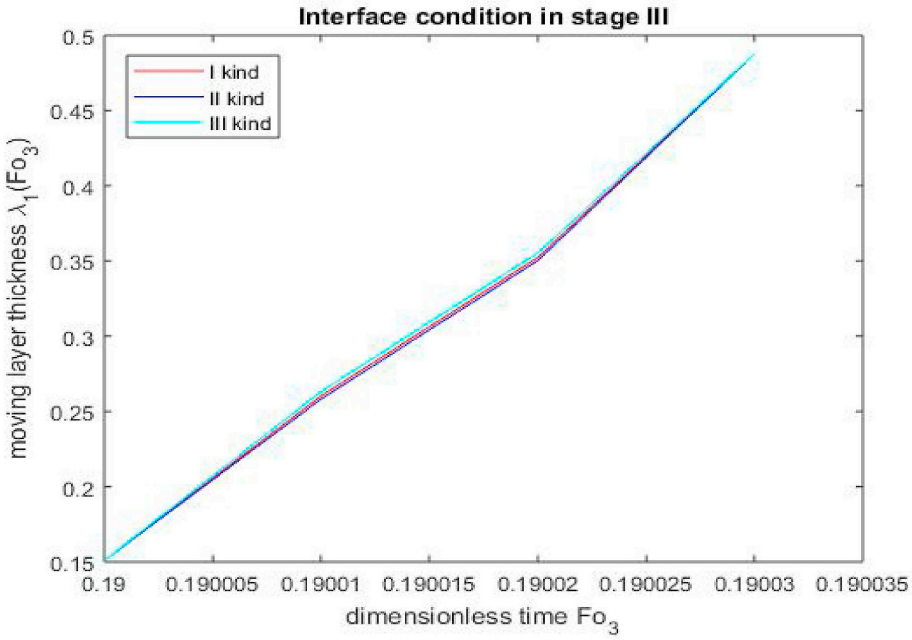

Fig. 8. Moving layer thickness λ_1 in stage3.

4.9. Stage 3

After solving Eqns (81), (97) and (100), we obtained

$$E_1 I + E_1 U_4{}'' \bar{P}\bar{\psi}(Fo_2^*)F - E_1 U_4{}''\bar{P} = \frac{B_i(\theta_w-\theta_r)}{h}H_1 - \frac{B_i(\theta_w-\theta_r)}{h}H_2 + \frac{B_i(\theta_w-\theta_r)}{k}H_1 - \frac{B_i(\theta_w-\theta_r)}{k}H_2 \quad (117)$$

After solving Eqns (82), (98) and (101), we obtained

$$\left(1-\frac{1}{Ste_3}\right)E_2 I + a_{23}E_2 U_5{}''\bar{P}\bar{\psi}(Fo_2^*)F - a_{23}E_2 U_5{}''\bar{P} = \frac{1}{(h^2+k^2)}H_2{}' \quad (118)$$

After solving Eqns (83), (99) and (102), we obtained

$$E_3 I + a_{13}E_3 U_6{}''\bar{P}\bar{\psi}(Fo_2^*)F - a_{13}E_3 U_6{}''\bar{P} = \frac{1}{(h^2+k^2)}H_3{}' \quad (119)$$

The problem in all the three Stages with different boundary condition converted into generalized system of Sylvester equations (90,95,96,103 − 117) whose solution is obtained by applying Bartels-Stewart algorithm (1972). And applying these results in interface condition, the position oayer thickness in Stage 2 and Stage 3 with generalized boundary condition determined. For numerical computation, Matlab Software is used.

5. Model verification for one-dimensional case

The exact solutions of equation (47- 56) are available for semi-

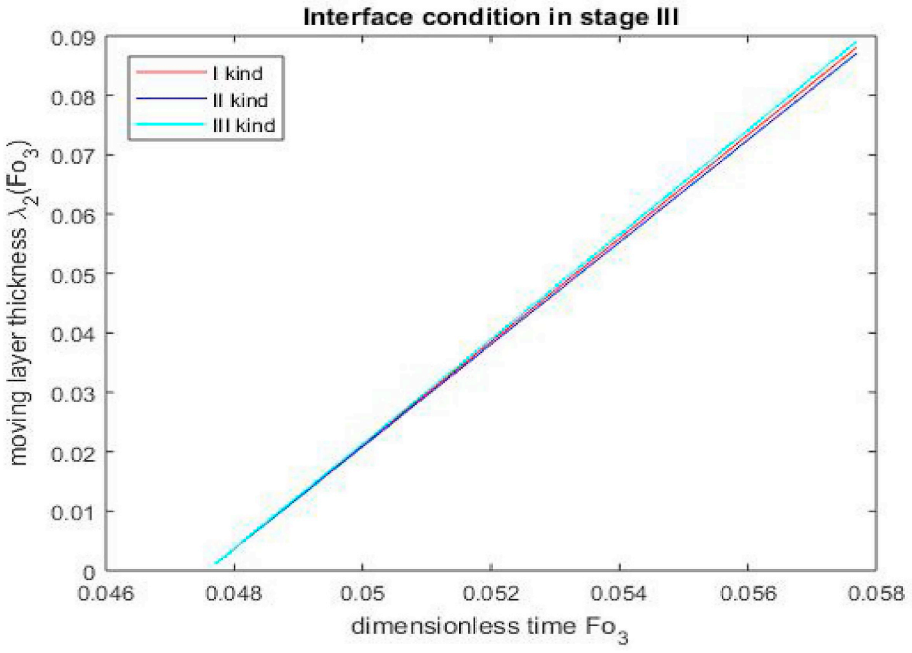

Fig. 9. Moving layer thickness λ_2 in stage3.

infinite one-dimension case. We have described the structure of one-dimensional problem in cryosurgery as a semi-infinite moving lte domain, which is initially in liquid phase at temperature T_0. The surface at $x = 0$ cooled by a cryoprobe at temperature T_c. The freezing starts and the domain is divided into three regions. In Stage 1 only unfrozen region is formed, in Stage 2 mushy and unfrozen regions are formed while in Stage 3 all the three regions: frozen, mushy and unfrozen are formed. We used Boundary fixation method to find the exact solution in Stage 3. Exact solution for this problem is as follows

$$\theta_f = -(C+4)i^2erfc(e_1 z) + Ci^2erfc(-e_1 z)$$

where

$$C = \frac{4i^2erfc(e_1)}{i^2erfc(-e_1) - i^2erfc(-e_1)}$$

$$\theta_m = \frac{erf\left(e_1 z\sqrt{\frac{1+\overline{Ste_3}}{a_{23}}}\right) - erf\left(e_1\sqrt{\frac{1+\overline{Ste_3}}{a_{23}}}\right)}{erf\left(e_2\sqrt{\frac{1+\overline{Ste_3}}{a_{23}}}\right) - erf\left(e_1\sqrt{\frac{1+\overline{Ste_3}}{a_{23}}}\right)}$$

and

$$\theta_u = 2 - \frac{erfc(e_1 z\sqrt{a_{13}})}{erfc(e_2\sqrt{a_{13}})}.$$

where

$\overline{Ste_3} = \frac{L}{c_m(T_s - T_l)}$, $a_{23} = \frac{a_2}{a_3}$, $a_{13} = \frac{a_1}{a_3}$, $z = \frac{X}{S_1}$, $e_1 = \frac{S_1}{2\sqrt{F_0}}$, e_2 =Modified $\frac{S_2}{2\sqrt{F_0}}$, $i^n erfc(x) = i^{n-1}\int_x^\infty erfc(t)dt$; $n = 0,1,2...$

Legendre wavelet Galerkin Method is presented in Section 5 of each Stage. The temperature was calculated by this method in all the three region. And with the help of temperature, we find the interface position. Figs. 2 and 3 show the temperature distribution and interface position calculated by Modified Legendre wavelet Galerkin Method, and their comparison with exact solutions. These Figs. 2 and 3 clearly demonstrate that numerical Modified Legendre wavelet Galerkin Method agrees completely with exact solution.

6. Result and discussion

In this paper, a two-dimensional mathematical model for the freezing of tumor tissue in lung is developed. The procedure of freezing is accomplished in three stages by imposing on it the boundary condition of I kind or II kind or III kind. For easy understanding of the model, we established the non-dimensional parameters described in section 3. Consequently, the dimensionless form of the model is described in Eqs. 26–42. We applied Modified Legendre wavelet Galerkin method (Kumar et al., 2018) in each phase of boundary condition I, II and III kind for the solution of a dimensionless model. In stage 2 and 3, the model is a moving boundary problem of partial differential equations. Eq. (39) shows the interface condition in stage 2 and Eq.(41,42) represent the interface condition in stage 3.We used interface condition of stage 2 and 3 to determine the moving layer thickness and obtain the values of $\lambda_2(Fo_2)$ in stage 2 and $\lambda_1(Fo_3)$, $\lambda_2(Fo_3)$ in stage 3. In both stages, the effect of Stefan number on Moving layer thickness is observed. Moving layer thickness increases as the Stefan number decreases. Also, the effect of Kirchoff number on moving layer thickness has been seen in Stage 3 of boundary condition II kind and the effect of Biot number on moving layer thickness has been seen in stage3 of boundary condition III kind. Moving layer thickness increases as the Kirchoff number increases and moving layer thickness decreases as the Biot number increases.Moving layer thickness and temperature distribution are two important factors during the cryosurgical treatment of lung tumor tissue for the prophecy of extreme damage to diseased tissue and the least damage to healthy lung tissue (Kumar et al., 2018). Consequently, we have analysed the temperature distribution in all stages with generalized boundary condition and moving layer thickness in the mushy and frozen region of boundary condition I, II and III kind.

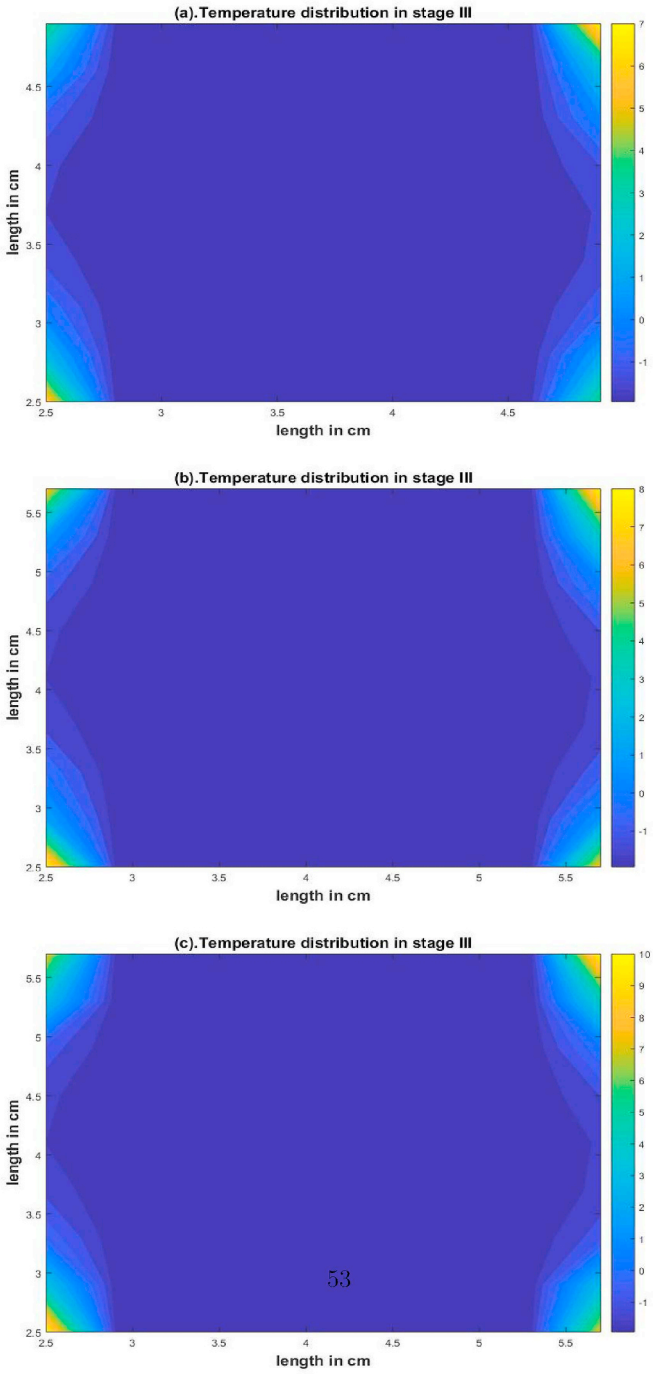

Fig. 10. Temperature distribution of unfrozen region in Stage3 at 900 s (a) I kind (b) II kind (c) III kind.

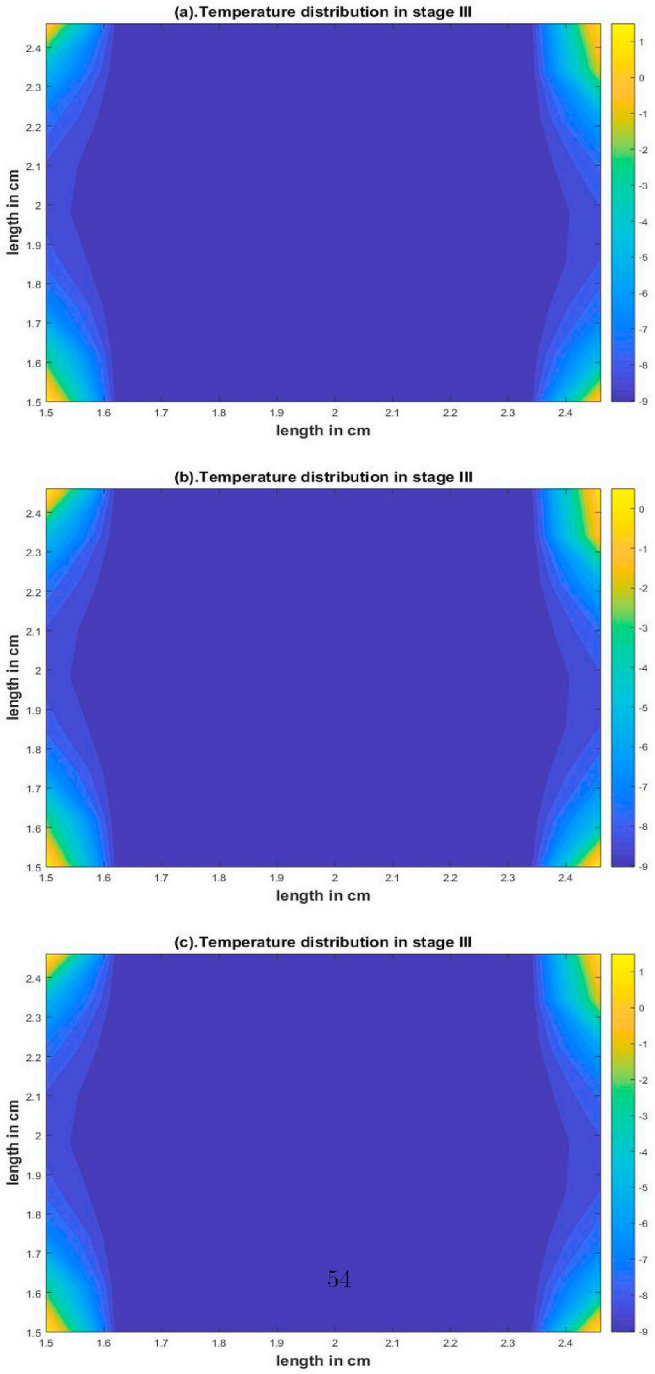

Fig. 11. Temperature distribution of mushy region in Stage3 at 900 s (a) I kind (b) II kind (c) III kind.

We have extracted the parameter of lung and tumor tissue for numerical computation from Table 1(Kumar et al., 2018; Katiyar et al., 2017; Bischof et al., 1992) given below:

Stage I:

Fig .4 exhibits the graph between temperature distribution and time for the generalized boundary condition in Stage I. In this stage, we see the temperature distribution at 200 s. In this figure(Fig. 4) we see the difference in the temperature distribution by keeping it at a constant temperature(I kind), a constant heat flux(II kind) and a constant heat transfer coefficient(III kind). We see how much temperature distribution vary by imposing boundary condition of I, II and III kind. In this stage, temperature decreases rapidly as the time increases. Here the lung tumor is cooled from initial temperature $T_0(37^0C)$ to liquidus temperature $T_l(-1^0C)$, and also the temperature (T_u) decreases as space coordinate x, y increases. We obtained the non-dimensional temperature Θ_u by applying Modified Legendre wavelet Galerkin Method and then obtained T_u.

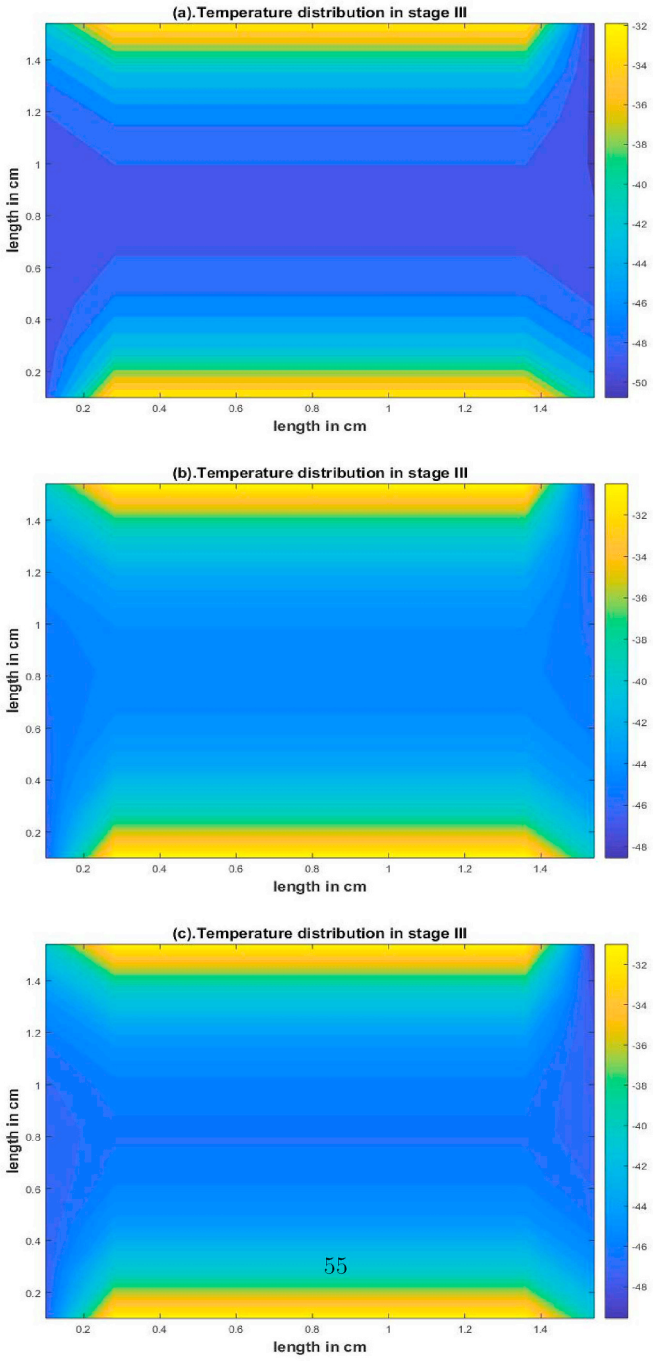

Fig. 12. Temperature distribution of frozen region in Stage3 at 900 s (a) I kind (b) II kind (c) III kind.

Stage II:

In this stage, Figs. 5 and 6 exhibits the graph between temperature distribution and time for the generalized boundary condition. In this stage, we see the temperature distribution at 500 s. In these figures (Figs. 5 and 6) we see the difference in the temperature distribution by keeping it at a constant temperature(I kind), a constant heat flux(II kind) and a constant heat transfer coefficient(III kind). We see how much temperature distribution vary by imposing boundary condition of I, II and III kind. As observed the temperature of unfrozen region diminishes slowly as compared to the mushy region. In this stage, the lung tumor is cooled from the liquidus temperature $T_l(-\ 1^0C)$ to solidus temperature $T_s(-\ 8^0C)$. We obtained the dimensionless temperature Θ_m and Θ_u by applying Modified wavelet Galerkin Method and then obtained T_m and T_u. We see that the temperature distribution in unfrozen (T_u) and mushy region(T_m) decreases as space coordinate x, y increases. We also see that there is slight variation not too much in temperature distribution by imposing generalized boundary condition (I, II and III kind). Fig. 7 shows the comparison of dimensionless moving layer thickness $\lambda_2(Fo_2)$ in the mushy-liquid region of boundary condition I, II and III kind and moving layer thickness $\lambda_2(Fo_2)$ increases as the dimensionless time Fo_2 increases. The effect of Stefan number on moving layer thickness is also observed in Fig. 13.

Stage III:

Here, the solidus moving front λ_1 and the liquidus moving front λ_2 are calculated. Fig. 8 exhibits the dimensionless moving layer thickness $\lambda_1(Fo_3)$ in solid-mush region and Fig. 9 exhibits the moving layer thickness $\lambda_2(Fo_3)$ in the mush-liquid region by imposing on it boundary condition of I, II and III kind. We see that $\lambda_1(Fo_3)$ and $\lambda_2(Fo_3)$ increases as the dimensionless time Fo_3 increases. Also, the effect of Stefan number is observed on moving layer thickness λ_1 and λ_2 in Figs. 14 and 15 respectively. We obtained the non-dimensional temperature Θ_f, Θ_m and Θ_u by applying Modified wavelet Galerkin Method and then obtained T_f, T_m and T_u. The temperature distribution in frozen region(T_f), mushy region(T_m) and unfrozen region(T_u) decreases as space coordinate x, y increases. Figs. 10–12 shows the graph between temperature distribution and time by keeping it at a constant temperature(I kind), a constant heat flux(II kind) and a constant heat transfer coefficient(III kind). In this stage, we see the temperature distribution at 900 s. In these figures, we see the difference in the temperature distribution of boundary condition I, II and III kind. We see how much temperature distribution vary with different boundary condition. As observed the temperature of the frozen region decreases rapidly as compared to the mushy region and the unfrozen region.

Figs. 8 and 9 exhibits the dimensionless moving layer thickness $\lambda_1(Fo_3)$ in the solid-mush region and $\lambda_2(Fo_3)$ in mush-liquid region respectively. As the time Fo_3 increases, moving layer thickness $\lambda_1(Fo_3)$ and $\lambda_2(Fo_3)$ increases. The effect of Stefan number on moving layer thickness is seen in Figs. 14 and 15. Also, the effect of the Kirchoff number and Biot number is seen in Figs. 16 and 17. Here the tissue is cooled from freezing temperature to the lethal temperature. In particular, the lethal temperature for tissue destruction usually begins around $-\ 40^0C$ (Zhang, 2009) for diseased tissue like a tumor.

7. Conclusion

In this study, a two-dimensional mathematical bio-heat transfer model of lung tumor tissue during the freezing process in cryosurgery has been developed and then used the Modified Legendre wavelets Galerkin method to obtain the results. Firstly, our problem is transformed into non-dimensional form and then applying finite difference method in our problem to convert it into initial boundary value problem of ordinary matrix differential equation in stage 1 and moving boundary value problem in stage 2 and 3 by imposing on it at a constant temperature(I kind), a constant heat flux(II kind) and a constant heat transfer coefficient(III kind) in each stage. After this, we obtained the system of Sylvester equations by using Legendre wavelet Galerkin

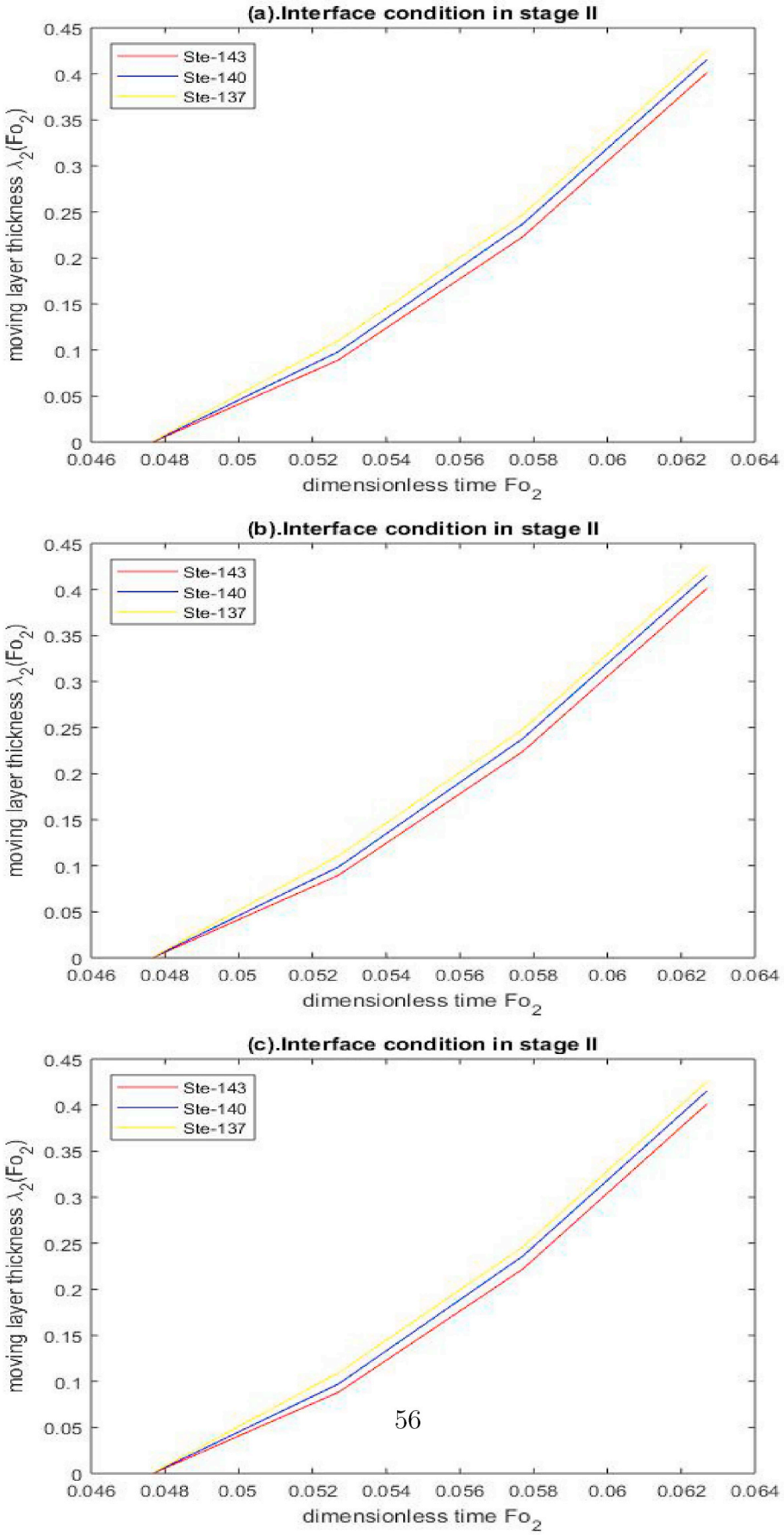

Fig. 13. Moving layer thickness λ_2 in stage2 with different Stefan number (a) I kind (b) II kind (c) III kind.

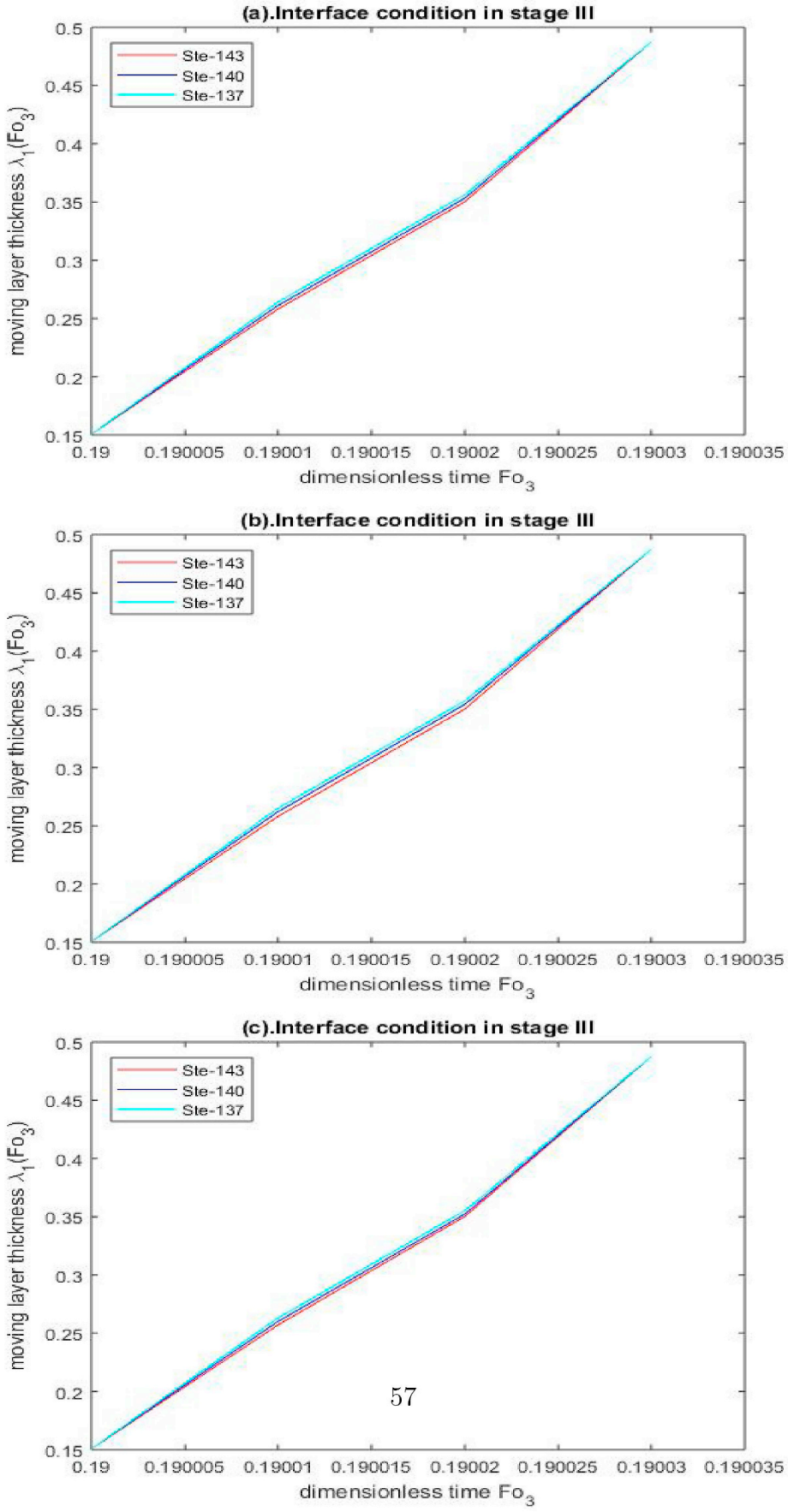

Fig. 14. Moving layer thickness λ_1 in stage3 with different Stefan number (a) I kind (b) II kind (c) III kind.

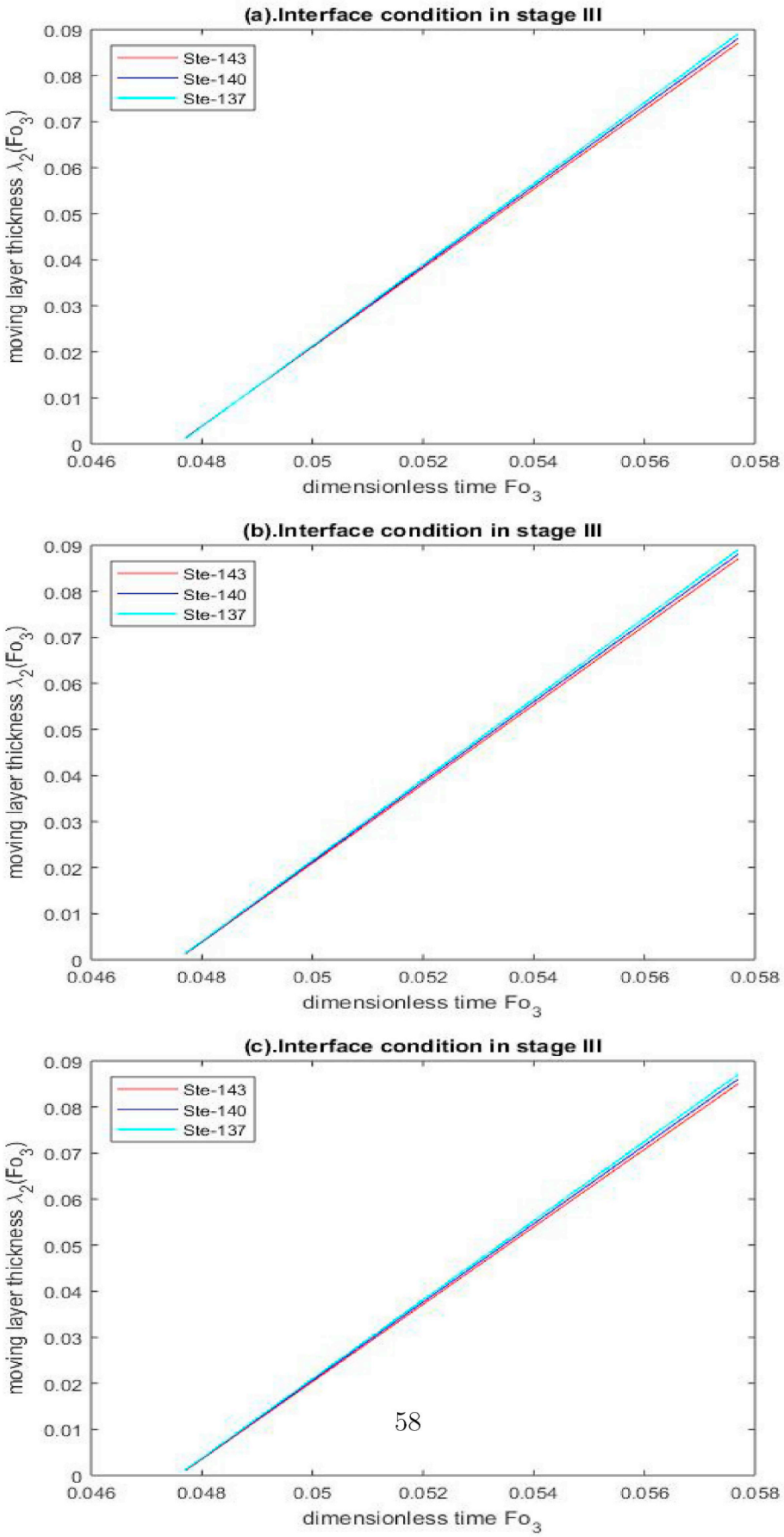

58

Fig. 15. Moving layer thickness λ_2 in stage3 with different Stefan number (a) I kind (b) II kind (c) III kind.

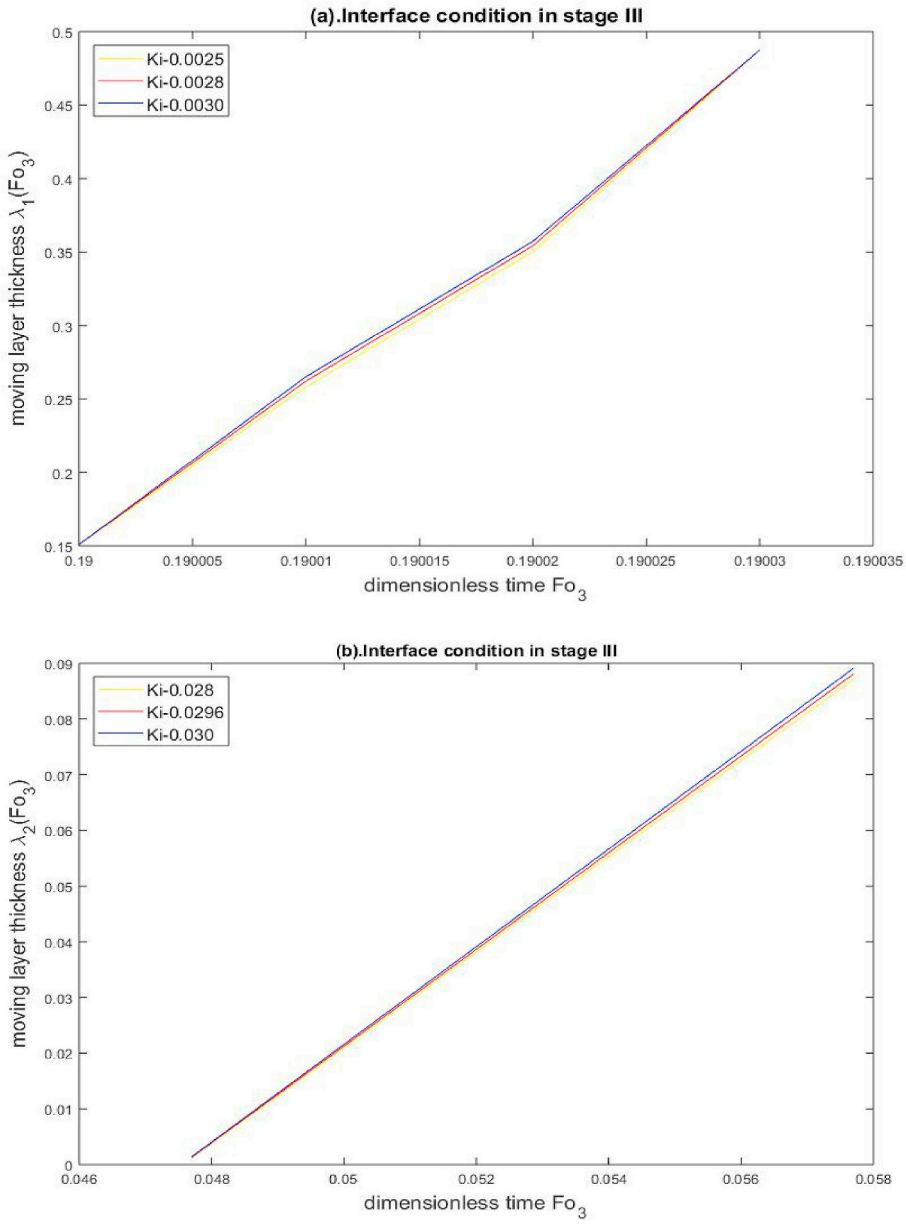

Fig. 16. Moving layer thickness in stage3 with different Kirchoff number (a).$\lambda_1(Fo_3)$ (b). $\lambda_2(Fo_3)$

method which are solved by generalized inverse technique (Bartels-Stewart algorithm). In each stage, we have applied this technique to carry out the temperature distribution. From our calculations, we see that the effect of relaxation time is negligible in the mushy and frozen region and present only in unfrozen region. We observe from the figures of moving layer thickness and temperature distribution that there is slight variation not too much with the effect of different boundary condition. In Stage1, the tissue is cooled up to the liquidus temperature $T_l(-1^0C)$ where unfrozen region is formed and then in Stage 2, the tissue is cooled up to the freezing temperature $T_s(-8^0C)$ where the mushy region is formed and in Stage3, the tissue is cooled up to the lethal temperature where the frozen region is formed. The effect of Stefan number on moving layer thickness is seen in stage 2 and 3. Also, the effect of Kirchoff number on moving layer thickness has been seen in Stage 3 of boundary condition II kind and the effect of Biot number on moving layer thickness has been seen in stage3 of boundary condition III kind. Moving layer thickness increases as the Kirchoff number increases and moving layer thickness decreases as the Biot number increases. Although a two-dimensional mathematical bio-heat transfer model is considered in our investigation, it can further be extended for

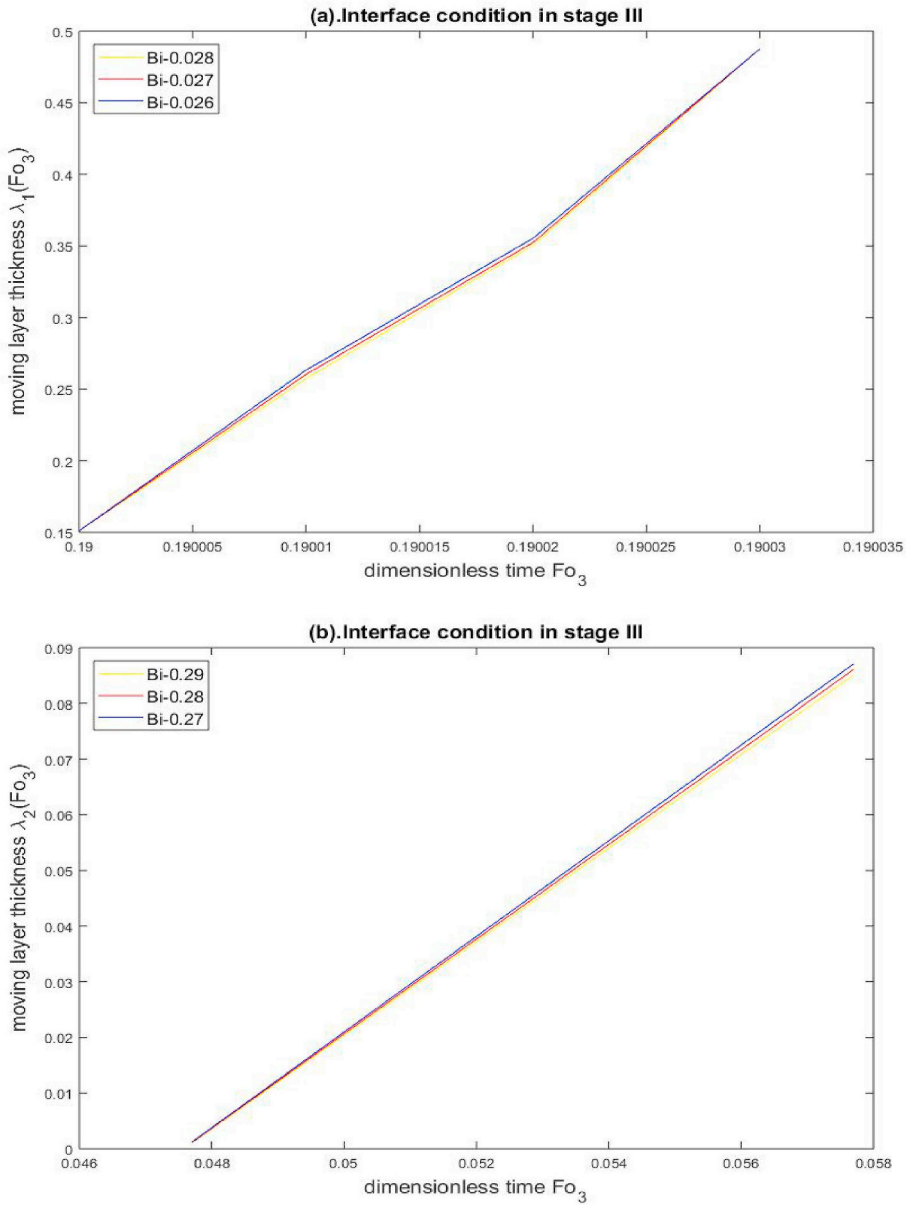

Fig. 17. Moving layer thickness in stage3 with different Biot number (a).$\lambda_1(Fo_3)$ (b). $\lambda_2(Fo_3)$

the three-dimensional mathematical bio-heat transfer model to attain more physically realistic results. Lastly, this model is beneficial for the experimental analysis of the freezing process of cryosurgical treatment.

Acknowledgments

The research of the first author is supported by University Grant Commission New Delhi, India, grant no. 19/06/2016(i)EU-V. The authors express their sincere thanks to DST-Centre for Interdisciplinary Mathematical Sciences, Banaras Hindu University Varanasi, India, for alloting the required facilities. The authors are grateful to the Reviewer for their valuable comments.

Appendix A. Supplementary data

Supplementary data to this article can be found online at https://doi.org/10.1016/j.jtherbio.2019.05.023.

References

Ahmadikia, H., Moradi, A., 2012. Non-Fourier phase change heat transfer in biological tissues during solidification. Heat Mass Transf. 48 (9), 1559–1568.
Allington, H.V., 1950. Liquid nitrogen in the treatment of skin diseases. Calif. Med. 72 (3), 153–155.
Antaki, P.J., 2005. New interpretation of Non-Fourier heat conduction in processed meat. ASME J. Heat Transf. 127, 189–193.
Bartels, R., Stewart, G., 1972. Solution of the matrix equation AX + XB = C: algorithm 432. Commun. ACM 15, 820–826.
Bischof, J.C., Bastacky, J., Rubinsky, B., 1992. An analytical study of cryosurgery in the lung. J. Biomech. Eng. 114 (4), 467–472.
Budman, H., Shitzer, A., Dayan, J., 1995. Analysis of the inverse problem of freezing and thawing of a binary solution durin cryosurgical processes. J. Biomech. Eng. 177, 193–202.
Cattaneo, C., 1958. A form of heat conduction equation which eliminates the paradox of instantaneous propagation. Comptes Rendus 247, 431–433.
Chua, K.J., Chou, S.K., Ho, J.C., 2007. An analytical study on the thermal effects of cryosurgery on selective cell destruction. J. Biomech. 40 (1), 100–116.
Deng, Z.S., Liu, J., 2005. Numerical simulation of selective freezing of target biological tissues following injection of solutions with specific thermal properties. Cryobiology 50 (2), 183–192.
Frayn, K.N., 1996. Metabolic Regulation: A Human Perspective. Portland Press, London, pp. 84–88.
Gupta, S.C., 2003. The Classical Stefan Problems: Basic Concepts,Modelling and Analysis.

Elsevier.
Islami, F., Goding Sauer, A., Miller, K.D., Siegel, R.L., Fedewa, S.A., Jacobs, E.J., McCullough, M.L., Patel, A.V., Ma, J., Soerjomataram, I., Flanders, W.D., Brawley, O.W., Gapstur, S.M., Jemal, A., January, 2018. Proportion and number of cancer cases and deaths attributable to potentially modifiable risk factors in the United States". CA 68 (1), 31–54. https://doi.org/10.3322/caac.21440. PMID 29160902.
Kotova, T.G., Kochenov, V.I., Tsybusov, S.N., Madai, D.Y., Gurin, A.V., 2016. Calculation of effective freezing time in lung cancer cryosurgery based on godunov simulation. CTM 8 (1).
Kumar, A., Kumar, S., Katiyar, V.K., Telles, S., 2017. Phase change heat transfer during cryosurgery of lung cancer using hyperbolic heat conduction model. Comput. Biol. Med. 84, 20–29 Math. Mech. 3 (3) (2007) 1–17.
Kumar, D., Singh, S., Rai, K.N., 2016. Analysis of classical fourier, SPL and DPL heat transfer model in biological tissues in presence of metabolic and external heat source. Heat Mass Transf. 52 (6), 1089–1107.
Kumar, Mukesh, Upadhyay, S., Rai, K.N., 2018. A study of cryosurgery of lung cancer using Modified Legendre wavelet Galerkin method. J. Therm. Biol. 78, 356–366.
Kumar, P., kumar, D., Rai, K.N., 2015. A numerical study on dual phase lag model of bio heat transfer during hyperthermia treatment. J. Therm. Biol. 49, 98–105.
Kumar, S., Katiyar, V.K., 2016. Numerical study on phase change heat transfer during combined hyperthermia and cryosurgical treatment of lung cancer. Int. J. Appl.
Lee, C.Y., Bastacky, J., 1995. Comparative mathematical analyses of freezing in lung and solid tissue. Cryobiology 32, 299–305.
Liu, K.C., Chen, H., 2009. Analysis for the dual-phase-lag bio-heat transfer during magnetic hyperthermia treatment. Int. J. Heat Mass Transf. 52, 1185–1192.
Majchrzak, E., 2010. Numerical solution of dual phase lag model of bioheat transfer using the general boundary element method. Comput. Model. Eng. Sci. 69 (1), 43–60.
Pasquali, Paola, Cryosurgery, 2015. Cryosurgery: A Practical Manual.
Pennes, H.H., 1948. Analysis of tissue and arterial blood temperatures in the resting human forearm. J. Appl. Physiol. 1 (2), 93–122.
Rabin, Y., Shitzer, A., 1995. Exact solution to the one-dimensional inverse-Stefan problem in non ideal biological tissue. J. Heat Transf. 117, 425–431.
Razzaghi, M., Yousefi, S., 2001. Legendre wavelets operational matrix of integration. Int. J. Syst. Sci. 32, 495–502.
Tarwidi, D., 2015. Godunov method for computerized lung cancer cryosurgery planning with efficient freezing time. In: Proceedings of the 3rd International Conference on IEEE the Information and Communication Technology (ICoICT), 2015, pp. 494–499.
Tolar, J., Neglia, J.P., June 2003. Transplacental and other routes of cancer transmission between individuals". J. Pediatr. Hematol. Oncol. 25 (6), 430–436. https://doi.org/10.1097/00043426-200306000-00002. PMID 12794519.
Tzou, D.Y., 1995. A unified field approach for heat conduction from macro to microscales. J. Heat Transf. 117, 8–16.
Yadav, S., Kumar, D., Rai, K.N., 2014. Finite Element Legendre Wavelet Galerkin Approach to inward solidification in simple body under most generalised boundary condition. Z. Naturforsch. 69a, 501–510.
Yadav, S., Upadhyay, S., Rai, K.N., 2016. A mathematical model for solidification of binary eutectic system including relaxation time. Comput. Therm. Sci. 8, 583–589.
Zhang, Y., 2009. Generalized dual-phase lag bio-heat equations based on non equilibrium heat transfer in living biological tissues. Int. J. Heat Mass Transf. 52, 4829–4834.
Zhou, J., Zhang, Y., Chen, J.K., 2009. An axisymmetric dual-phase-lag bioheat model for laser heating of living tissues. Int. J. Therm. Sci. 48, 1477–1485.